



RESEARCH ARTICLE

10.1002/2016GB005372

Key Points:

- Aggregate sinking speeds are controlled by processes in the plankton community
- Plankton communities can affect sinking speed by altering aggregate porosity and ballasting
- *Emiliana huxleyi* blooms of 1500 cells/mL increase organic matter transfer efficiency from 14 to 24%

Supporting Information:

- Supporting Information

Correspondence to:

L. T. Bach,
lbach@geomar.de

Citation:

Bach, L. T., T. Boxhammer, A. Larsen, N. Hildebrandt, K. G. Schulz, and U. Riebesell (2016), Influence of plankton community structure on the sinking velocity of marine aggregates, *Global Biogeochem. Cycles*, 30, 1145–1165, doi:10.1002/2016GB005372.

Received 5 JAN 2016

Accepted 6 JUL 2016

Accepted article online 9 JUL 2016

Published online 13 AUG 2016

Influence of plankton community structure on the sinking velocity of marine aggregates

L. T. Bach¹, T. Boxhammer¹, A. Larsen², N. Hildebrandt³, K. G. Schulz^{1,4}, and U. Riebesell¹

¹GEOMAR Helmholtz Centre for Ocean Research Kiel, Kiel, Germany, ²Hjort Centre for Marine Ecosystem Dynamics, Uni Research Environment, Bergen, Norway, ³Alfred Wegener Institute Helmholtz Centre for Polar and Marine Research, Bremerhaven, Germany, ⁴Centre for Coastal Biogeochemistry, Southern Cross University, East Lismore, New South Wales, Australia

Abstract About 50 Gt of carbon is fixed photosynthetically by surface ocean phytoplankton communities every year. Part of this organic matter is reprocessed within the plankton community to form aggregates which eventually sink and export carbon into the deep ocean. The fraction of organic matter leaving the surface ocean is partly dependent on aggregate sinking velocity which accelerates with increasing aggregate size and density, where the latter is controlled by ballast load and aggregate porosity. In May 2011, we moored nine 25 m deep mesocosms in a Norwegian fjord to assess on a daily basis how plankton community structure affects material properties and sinking velocities of aggregates (Ø 80–400 µm) collected in the mesocosms' sediment traps. We noted that sinking velocity was not necessarily accelerated by opal ballast during diatom blooms, which could be due to relatively high porosity of these rather fresh aggregates. Furthermore, estimated aggregate porosity ($P_{\text{estimated}}$) decreased as the picoautotroph (0.2–2 µm) fraction of the phytoplankton biomass increased. Thus, picoautotroph-dominated communities may be indicative for food webs promoting a high degree of aggregate repackaging with potential for accelerated sinking. Blooms of the coccolithophore *Emiliana huxleyi* revealed that cell concentrations of ~1500 cells/mL accelerate sinking by about 35–40%, which we estimate (by one-dimensional modeling) to elevate organic matter transfer efficiency through the mesopelagic from 14 to 24%. Our results indicate that sinking velocities are influenced by the complex interplay between the availability of ballast minerals and aggregate packaging; both of which are controlled by plankton community structure.

1. Introduction

Phytoplankton fixes approximately 50 Gt of carbon in the euphotic zone of the oceans every year [Longhurst *et al.*, 1995; Field *et al.*, 1998]. Most of this organic carbon is remineralized in the surface ocean. However, 5–12 Gt C escape remineralization and are exported out of the surface (100 m), either as dissolved organic carbon (DOC) trapped in downwelling water currents, as particulate organic carbon (POC) sinking due to gravity, or transported downward by vertically migrating zooplankton [Hansell and Carlson, 2001; Turner, 2002; Honjo *et al.*, 2008; Steinberg *et al.*, 2008; Henson *et al.*, 2011; Siegel *et al.*, 2014]. A large fraction of the POC and DOC is biologically remineralized during its descent through subsurface water and released as dissolved inorganic carbon (DIC). That way, DIC is transported from surface to depth against a concentration gradient in a series of biologically mediated processes—the reason why this has been termed the biological pump [Volk and Hoffert, 1985]. A shutdown of the biological pump would lead to a significant accumulation of DIC in the surface ocean paralleled by a roughly 60–70% increase of current atmospheric CO₂ concentrations within a 1000 year equilibration time [Maier-Reimer *et al.*, 1996]. This highlights the outstanding importance of the biological pump for the global carbon cycle and climate.

The fraction of surface-originating POC that reaches the deep ocean depends on the balance between particle remineralization rates and sinking velocities. A fast-sinking particle made of relatively refractory POC will experience little remineralization during its descent from the euphotic zone (~0–200 m) through the mesopelagic (200–1000 m) into the deep ocean (below 1000 m). Conversely, a slowly sinking particle made of labile and easily disintegrating POC would never reach that far. Remineralization rates are controlled by bacterial activity and mesozooplankton feeding as well as particle fragmentation rates [Kjørboe, 2001; Giering *et al.*, 2014]. Sinking velocity is determined by the viscosity of seawater, particle size, shape, and excess density [Stokes, 1850; McNown and Malaika, 1950; Smayda, 1970], where the latter depends primarily on porosity of the particle and the amount of ballast mineral attached to it [Alldredge and Gotschalk, 1988].

Opal, CaCO_3 , and lithogenic minerals are ballast materials formed in or deposited onto the oceans' surface layer. Opal is formed by diatoms, silicoflagellates, and radiolarians, while CaCO_3 is mainly formed by coccolithophores, calcifying dinoflagellates, foraminifera, and pteropods. Lithogenic minerals are usually of terrigenous origin and transported into the oceans via dust events or river input. Ballast minerals are important components in particle export as they may slow down remineralization of associated POC [Hedges and Oades, 1997] and increase particle excess density, thereby accelerating sinking velocity [e.g., Passow and De La Rocha, 2006; Honjo et al., 2008; Ploug et al., 2008]. These mechanisms were used to explain the ballast ratio hypothesis [Armstrong et al., 2009], which originates from the observation that globally averaged POC: ballast mineral ratios are high and variable in the euphotic zone but converge to relatively narrow and stable values in the deep [Armstrong et al., 2002]. The ballast ratio hypothesis suggests that ballast minerals, in particular relatively dense CaCO_3 , strongly support deep ocean POC sequestration since most organic material reaching below 2000 m is associated with them [Francois et al., 2002; Klaas and Archer, 2002].

Recently, however, the ballast ratio hypothesis has been called into question. Passow and De La Rocha [2006] and Boyd and Trull [2007] noted that globally averaged correlations between ballast materials and POC may not be found on regional scales or along the course of an entire seasonal cycle. This concern was confirmed by the analysis of Wilson et al. [2012] and Le Moigne et al. [2014], who found variable regional correlations between CaCO_3 and POC in the deep and in the surface ocean and consequently attributed the tight global correlation as an artifact of spatial averaging. Francois et al. [2002], Lam and Bishop [2007], Lam et al. [2011], and Henson et al. [2012a, 2012b] reported that ballast-rich diatom blooms are characterized by surprisingly low POC transfer efficiencies into the deep ocean and explained this finding by (1) the high degree of fluffiness of diatom aggregates and (2) the relatively large proportion of easily degradable organic carbon compounds within diatom aggregates. In consequence, they suggested that POC transfer efficiency is not primarily determined by the presence of ballast minerals but by the upper ocean ecosystem structure with those systems producing tightly packed and refractory aggregates having highest transfer efficiencies. It is important to keep in mind, however, that these recent developments do not exclude an important influence of ballast under all circumstances. Instead, they shift the focus from ballast materials as primary controlling factor of export toward the state of the pelagic ecosystems being of major relevance for export flux. Nevertheless, ballast materials may seasonally and/or regionally still be very important [e.g., Waite et al., 2005; Honda and Watanabe, 2010; Martin et al., 2011; Smetacek et al., 2012].

In this study we used mesocosms to follow the development of particle sinking velocities over time and connect it to the succession of natural plankton communities in order to evaluate the influence of food web processes on sinking.

2. Materials and Methods

2.1. Experimental Setup

In May 2011, nine "Kiel Off-Shore Mesocosms for future Ocean Simulations" (M1–M9) were deployed for 5 weeks in a Norwegian fjord (Raunefjord; 60.265°N, 5.205°E) close to the city of Bergen. The cylindrical but initially folded mesocosm bags made of transparent polyurethane foil were mounted in 8 m long floating frames [Riebesell et al., 2013]. After mooring of the flotation frames at the study site, bags were unfolded by lowering the bottom part to 24 m, thereby enclosing the natural plankton community. Bottom and top of the cylindrical bags were covered with 3 mm meshes before extension to exclude patchily distributed larger plankton (e.g., adult jelly fish) and nekton (e.g., fish). The mesh-covered mesocosms were allowed to exchange with seawater for 3 days. After this period, scuba divers closed the mesocosms by removing the bottom mesh and then quickly sealing the wide opening with a 2 m long conical sediment trap. The upper openings of the bags were pulled above the water surface directly after trap attachment, thereby isolating the enclosed plankton community from the surrounding fjord water. The mesh covering the upper opening was removed thereafter.

All mesocosms were 25 m deep (Figure 1), 2 m in diameter, and contained a volume of approximately 75 m³. Sampling started after the mesocosms were closed, and the water column was mixed for 5 min by bubbling with compressed air eliminating a slight salinity stratification [Riebesell et al., 2013]. Salinity was ~32 throughout the entire water column after mixing and decreased to ~31.9 at the end of the experiment due to dilution

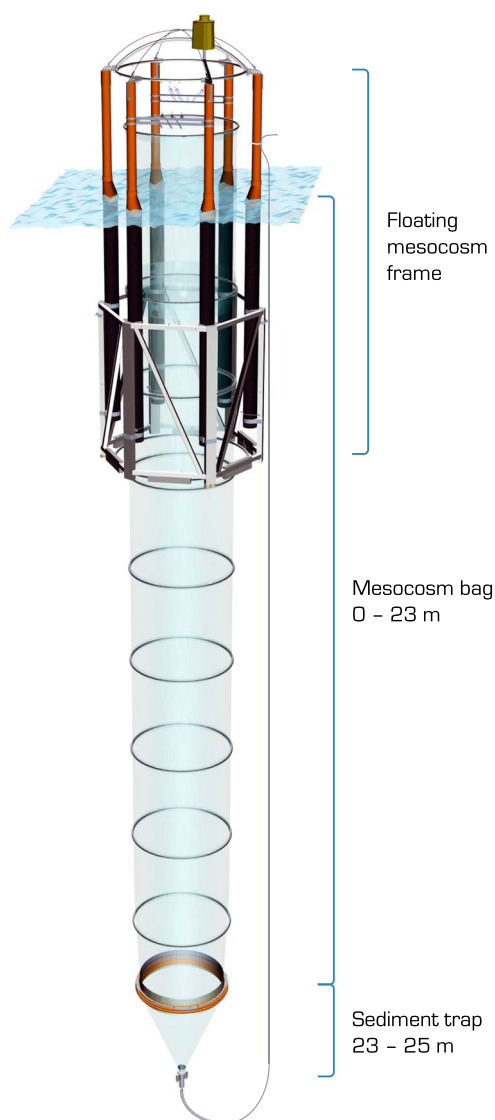


Figure 1. Schematic drawing of the KOSMOS system [Riebesell *et al.*, 2013]. The video by Boxhammer *et al.* [2015] gives an impression on the plankton community enclosed in these mesocosms.

with the trigger set on red fluorescence [Larsen *et al.*, 2001]. Light microscopy investigations revealed that hardly any phytoplankton cells $>50\ \mu\text{m}$ were present in the samples, making the flow cytometry measurements (covering the size range $<100\ \mu\text{m}$) representative for the overall size spectrum. Subsamples for chlorophyll *a* and BSi were filtered with gentle vacuum (200 mbar) on glass fiber filters or cellulose acetate filters, respectively. Both sample types were stored at -20°C until measurements following Welschmeyer [1994] (chlorophyll *a*) or Hansen and Koroleff [1999] (BSi). Nitrate (NO_3^-), phosphate (PO_4^{3-}), and silicate (Si(OH)_4) concentrations were determined following Hansen and Koroleff [1999] using a Hitachi U2000 spectrophotometer [Schulz *et al.*, 2013].

Zooplankton samples were collected with an Apstein net (55 μm mesh size, 0.17 m net opening) on a weekly basis. The maximum sampling depth was 23 m to prevent any contact of the net with the sediment trap. Sampling was restricted to four net hauls per mesocosm and week in order to avoid overfishing. Zooplankton were transported to the lab in less than an hour, where it was preserved with hexamethylenetetramine-buffered formalin (4% (v/v)) for counting and taxonomic analyses with a stereomicroscope.

by rainwater. All mesocosms were left unperturbed for the first 4 days of the experiment. Subsequently, seven of them were enriched with different amounts of CO_2 -saturated seawater as explained by Riebesell *et al.* [2013] to reach initial $p\text{CO}_2$ levels of 300, 310 (both untreated controls), 395, 590, 890, 1165, 1425, 2060, and 3045 μatm . The mesocosm with 300 μatm (M2) was discovered to have an unmendable hole and was thus excluded from analyses. All mesocosms were enriched with $\sim 5\ \mu\text{mol L}^{-1}\ \text{NO}_3^-$ and $\sim 0.16\ \mu\text{mol L}^{-1}\ \text{PO}_4^{3-}$ in the middle of the experiment (Julian day 142; 22 May) as described by Schulz *et al.* [2013].

2.2. Sampling and Processing of Water Column Parameters

Phytoplankton, particulate matter, and dissolved inorganic nutrient samples were taken every morning between 09:00 and 11:00 A.M. with integrating water samplers (Hydro-Bios), which collect equal amounts of water from every depth (0–23 m). Depth-integrated samples were stored in 10 L carboys, transported to land, and kept in the dark at in situ temperature until subsampling for flow cytometry, chlorophyll *a*, biogenic silica (BSi), and inorganic nutrients. Great care was taken to mix the carboys before every subsampling. The time between mesocosm sampling and subsampling from the carboys was usually well below 3 h. Flow cytometry subsamples (50 mL) were stored at in situ temperature for a maximum of 3 h until analysis with a FACSCalibur flow cytometer (BD Biosciences). Phytoplankton enumerations were obtained from fresh samples based on difference in chlorophyll autofluorescence and side scatter

2.3. Sampling and Processing of Sediment Trap Material

The bottom of the mesocosms had the conical shape of a sediment trap (Figure 1). Sinking material collected in the traps was pumped daily between 08:00 and 09:00 A.M. through a 25 m long (10 mm inner diameter) silicon tube under low vacuum into a glass bottle at the surface [Boxhammer *et al.*, 2016]. The bulk of the sediment trap material (>97%) was used to determine the amount and composition of particulate matter, while small subsamples were used for zooplankton counting and particle sinking velocity measurements (see below).

Bulk samples were concentrated by centrifugation. Resulting pellets were freeze-dried, weighed, and ground to fine powder as described by Boxhammer *et al.* [2016]. The powder was used for POC, total particulate carbon (TPC), and BSi measurements. Before analysis, POC samples were soaked with 50 μL of 1 molar HCl to remove all CaCO_3 . TPC and POC samples were subsequently analyzed on a C/N elemental analyzer (Hekatech). Particulate inorganic carbon (PIC) was calculated from the difference of TPC and POC. The amount of sediment trap BSi was measured photometrically according to Hansen and Koroleff [1999].

Results from PIC, POC, and BSi analyses were used to estimate the relative contribution of each of these constituents to the material weight of the collected aggregates excluding water. Therefore, we assumed (1) material weights ($\text{weight}_{\text{material}}$) of 1.06, 2.1, and 2.7 g cm^{-3} for POM, BSi, and PIC, respectively [Sarmiento and Gruber, 2006] and (2) that no components other than these three contributed to the weight of the collected material. Assumption 2 is reasonable because there was no significant source of lithogenic ballast materials inside a mesocosm, and all lithogenic particles present at the beginning of the experiment should sink out during the first days (see section 4.2.1). Accordingly, the contribution of biogenic materials to the total material weight ($\text{weight}_{\text{fraction}}$) is calculated as

$$\text{weight}_{\text{fraction}} = \frac{b \times \text{weight}_{\text{material}}}{1.06 \times \text{POC} + 2.1 \times \text{BSi} + 2.7 \times \text{PIC}} \quad (1)$$

where b is either POM, BSi, or PIC and $\text{weight}_{\text{material}}$ is their respective densities.

Zooplankton samples (10 mL) were transferred into glass vials and preserved with hexamethylenetetramine-buffered formalin (4% (v/v)). Samples from two consecutive days but from the same mesocosm were then pooled and subsequently analyzed with a stereomicroscope.

Samples for sinking velocity measurements were carefully sieved (300 μm) to exclude very large gelatinous zooplankton, which can (when present) clog the settling column [Bach *et al.*, 2012a]. Samples were diluted with filtered (0.2 μm) seawater (salinity ~ 33.7) to keep particle concentrations low enough to avoid particle-particle interactions in the settling column, which are known to accelerate sinking velocities [Bach *et al.*, 2012a]. This preparation procedure had little effect on fecal pellet integrity, and we also did not observe that pellets were retained on the sieve [Bach *et al.*, 2012a]. Fluffy aggregates, however, did most likely not maintain their original size during sampling preparation. Instead, they continuously disintegrated and re-aggregated so that their size, density, and porosity measured in the settling column are potentially different than they were when they were sinking in situ. The methodological uncertainties will be outlined in section 2.5, and limitations will be further discussed in section 4.2.2.

2.4. Particle Sinking Velocity and Size Measurements

Sinking velocities of the sediment trap samples were measured directly after preparation for ~ 20 min with the FlowCam method described in Bach *et al.* [2012a]. This camera-based method allows parallel measurements of sinking velocity, equivalent spherical diameter (ESD), and shape of each particle sinking through the settling chamber. Turbulence within the settling column induced by convection was suppressed by operating the system in a temperature-controlled room (10°C) and constantly ventilating the settling chamber [Bach *et al.*, 2012a]. The size of the settling column is relatively small (400 mm long \times 10 mm wide \times 3 mm deep) due to technical restrictions of the camera. This also limits the size of aggregates that can be reasonably investigated to a maximum of 400 μm , because significantly larger aggregates would experience too pronounced wall effects. Sinking aggregates were divided in four size classes according to their ESD to facilitate data evaluation and discussion. Size classes were 80–130 μm , 120–180 μm , 170–260 μm , and 240–400 μm . The slight overlap between them was necessary to avoid exclusion of aggregates with an ESD exactly on the border of two size classes [Bach *et al.*, 2012a].

2.5. Aggregate Density and Porosity Calculations

Aggregate density ($\rho_{\text{aggregate}}$) was calculated from measured sinking velocity (U_{measured}) and ESD using Stokes' law:

$$\rho_{\text{aggregate}} = \frac{U_{\text{measured}} \times \mu_{\text{seawater}}}{\frac{2}{9} \times g \times \left(\frac{\text{ESD}}{2}\right)^2} + \rho_{\text{seawater}} \quad (2)$$

where g is the Earth's gravitational acceleration, ESD is the equivalent spherical diameter of the aggregate, μ_{seawater} is the viscosity of seawater, and ρ_{seawater} is the density of seawater. The μ_{seawater} and ρ_{seawater} were calculated from known salinity and temperature with the equations provided by *Sharqawy et al.* [2010].

The application of Stokes' law for calculations of $\rho_{\text{aggregate}}$ is appropriate when particles are equiaxial and sink in a laminar flow regime. Laminar flow was established in our measurements since investigated particles sank sufficiently slow and were relatively small so that their Reynolds numbers always remained far below the critical threshold of 0.5 [*McNown and Malaika*, 1950]. Aggregate shape was random but the aspect ratio (i.e., length/width) of the majority of aggregates was above 0.8, also indicating a higher abundance of debris relative to fecal pellets. We therefore consider particle shape and orientation while sinking to be of relatively small influence since shape only becomes an important factor when width deviates considerably from length [*McNown and Malaika*, 1950].

We propagated assumed imprecision of 5% in U_{measured} , 2% in ESD, 0.1% in ρ_{seawater} , and μ_{seawater} in equation (2) to assess the statistical error in $\rho_{\text{aggregate}}$. This analysis suggests an error of around 0.0012 g cm^{-3} in $\rho_{\text{aggregate}}$, which is small compared to absolute $\rho_{\text{aggregate}}$ values. However, in the context of sinking velocity, it is necessary to consider changes in excess density (i.e., $\rho_{\text{aggregate}} - \rho_{\text{seawater}}$). For the latter, we estimated a statistical error of $\sim 0.0016 \text{ g cm}^{-3}$ based on the abovementioned individual imprecisions in $\rho_{\text{aggregate}}$ and ρ_{seawater} . This resulted in a relative error (i.e., 0.0016 g cm^{-3} divided by absolute excess density) between 6 and 40%, which increased with decreasing $\rho_{\text{aggregate}}$.

Porosity is the fraction of an aggregate not occupied by solid matter [*Allredge and Gotschalk*, 1988]. Assuming that the investigated aggregate had no porosity, then its theoretical density (ρ_{theo}) would be

$$\rho_{\text{theo}} = 1.06 \times \text{frac}_{\text{POC}} + 2.1 \times \text{frac}_{\text{BSi}} + 2.7 \times \text{frac}_{\text{PIC}} \quad (3)$$

where frac_{POC} , frac_{BSi} , and frac_{PIC} are the relative contribution of each of the three materials to the total weight (equation (1)). An aggregate with a theoretical density between 1.06 (pure POC) and 2.7 g cm^{-3} (pure CaCO_3) will then have to be "diluted" with seawater ($\rho_{\text{seawater}} 1.025 \text{ g cm}^{-3}$) to such a degree that ρ_{theo} plus ρ_{seawater} equals $\rho_{\text{aggregate}}$ or

$$\rho_{\text{aggregate}} = \frac{\rho_{\text{theo}} + u \times \rho_{\text{seawater}}}{u + 1} \quad (4)$$

where u is the dilution factor. Solving equation (4) for u yields

$$u = \frac{\rho_{\text{theo}} - \rho_{\text{aggregate}}}{\rho_{\text{aggregate}} - \rho_{\text{seawater}}} \quad (5)$$

Porosity estimates ($P_{\text{estimated}}$) were subsequently calculated as

$$P_{\text{estimated}} = 1 - \frac{1}{u + 1} \quad (6)$$

Potential imprecisions in density variables will also be reflected in the precision of $P_{\text{estimated}}$. We estimated a statistical imprecision of $\sim 40 \text{ g cm}^{-3}$ in ρ_{theo} based on assumed imprecisions of 5% in the theoretical density of POC [*Bach et al.*, 2012a], as well as 2% in frac_{POC} , frac_{BSi} , and frac_{PIC} , respectively. This, together with the abovementioned error in $\rho_{\text{aggregate}}$ and ρ_{seawater} lead to a statistical imprecisions between 2 and 30 in the dilution factor u (Δu). Lower Δu coincided with lower absolute values in u , which explains why the absolute imprecision in $P_{\text{estimated}}$ is decreasing with increasing Δu . For example, we estimated that $P_{\text{estimated}}$ ranges between 0.985 and 0.992 when u is 100 and Δu is 30, while it ranges between 0.909 and 0.933 when u is 12 and Δu is 2 (equation (6)). This analysis indicates that the imprecision in $P_{\text{estimated}}$ is generally smaller than the changes observed in the course of the study, although it can be in the same range in some occasions (as exemplified in the second case described in the previous sentence). Aggregate fragmentation and

reassembly through sample treatment before measurements (see section 2.3) was another potential source of error in $\rho_{\text{aggregate}}$ and hence $P_{\text{estimated}}$. This aspect will be addressed in section 4.2.2.

A critical assumption for the accuracy of the porosity calculation is the equality of chemical composition in all aggregate size classes. Deviations could for instance arise from large numbers of mesozooplankton in the traps, which may bind an increased fraction of the POC in a particular size class. Mesozooplankton, however, was far less visible than phytodetritus, which strongly dominated the sediment trap material until the end of this investigation (appearance of sediment trap material shown in Figure S1 in the supporting information). Although we cannot entirely rule out the possibility of systematic changes in composition with size, there are three lines of evidence indicating that this was rather not the case: (1) large aggregates are composed of smaller aggregate building blocks [Kjørboe, 2001; Burd and Jackson, 2009] so that variability in chemical composition should average out unless the aggregate is composed of a single component [Alldredge, 1998]; (2) sinking velocity and $\rho_{\text{aggregate}}$ showed very similar trends in all four size classes, suggesting that particle properties do not systematically change with size (section 3.2); and (3) while filming the sinking particles with the microscope camera (FlowCam), we noted that the aggregate matrix appeared fairly homogenous among the size classes (Figure S1).

2.6. Assessment of Transfer Efficiency

Transfer efficiency is defined as the ratio of sequestration flux to export flux, where the former is the amount of sinking matter reaching the bottom of the mesopelagic zone (i.e., 1000 m) and the latter the amount reaching the bottom of the euphotic zone (see Sanders *et al.* [2014] for definitions). Sinking velocities of surface ocean aggregates as determined in this study cannot be used directly to derive transfer efficiencies. We therefore formulated a simple one-dimensional carbon flux model in order to test whether the magnitude of change in measured sinking velocities could affect transfer efficiency.

Key assumptions for the one-dimensional model are (1) the depth of the euphotic zone is 100 m and particles passing this depth enter the export pathway, (2) lateral POC inputs or losses below the euphotic zone are balancing each other, and (3) particle remineralization (k_{remin} (day^{-1})) during sinking is parameterized as a function of temperature (T in $^{\circ}\text{C}$) according to Schmittner *et al.* [2008]:

$$k_{\text{remin}} = 0.048 \times 1.066^{T(z)} \quad (7)$$

where z is the depth in meters. This equation accounts for a doubling of enzymatic activity for a 10° increase of temperature (Q_{10} kinetics). For $T(z)$ we used the average profile at 61.5°N between 16 and 17°W from July 2013 downloaded from the world ocean atlas data set (<https://www.nodc.noaa.gov/OC5/indprod.html>), which is an open ocean region but approximately the same latitude as our study site. (4) Model sinking velocity (m d^{-1}) is parameterized as

$$U_{\text{model}} = 0.04z + 25 \quad (8)$$

The stepwise increase in U_{model} is explained with a loss of the organic carbon content in aggregates [Berelson, 2002]. Note that this parameterization was adopted from the University of Victoria model [Schmittner *et al.*, 2008], but the sinking velocity at the surface was changed from 7 m d^{-1} [as in Schmittner *et al.*, 2008] to 25 m d^{-1} in order to receive a transfer efficiency of $\sim 14\%$ between 100 and 1000 m depth in the control run, which corresponds to a Martin b of about 0.85 [Martin *et al.*, 1987]. This value is around the average flux attenuation among different ocean basins [Berelson, 2001]. (5) The POC fraction which is remineralized on every depth interval depends on the balance between remineralization rates and sinking velocities. With these assumptions we can formulate the one-dimensional carbon flux model as

$$\text{POC}(z) = \text{POC}(z-1) - \left(\text{POC}(z-1) \times \frac{k_{\text{remin}}}{U_{\text{model}}} \times [z - (z-1)] \right) \quad (9)$$

where $z-1$ is the depth interval above the calculated depth.

The sinking velocity term (U_{model} ; equation (8)) was then multiplied with a stepwise increasing factor in order to simulate an acceleration of aggregate sinking speed over the entire water column. The corresponding increase of transfer efficiency of POM (in percent) between the bottom of the euphotic zone (here 100 m) and 1000 m was calculated for each multiplication step as

$$\text{Transfer efficiency} = \frac{\text{POM}_{1000}}{\text{POM}_{100}} \quad (10)$$

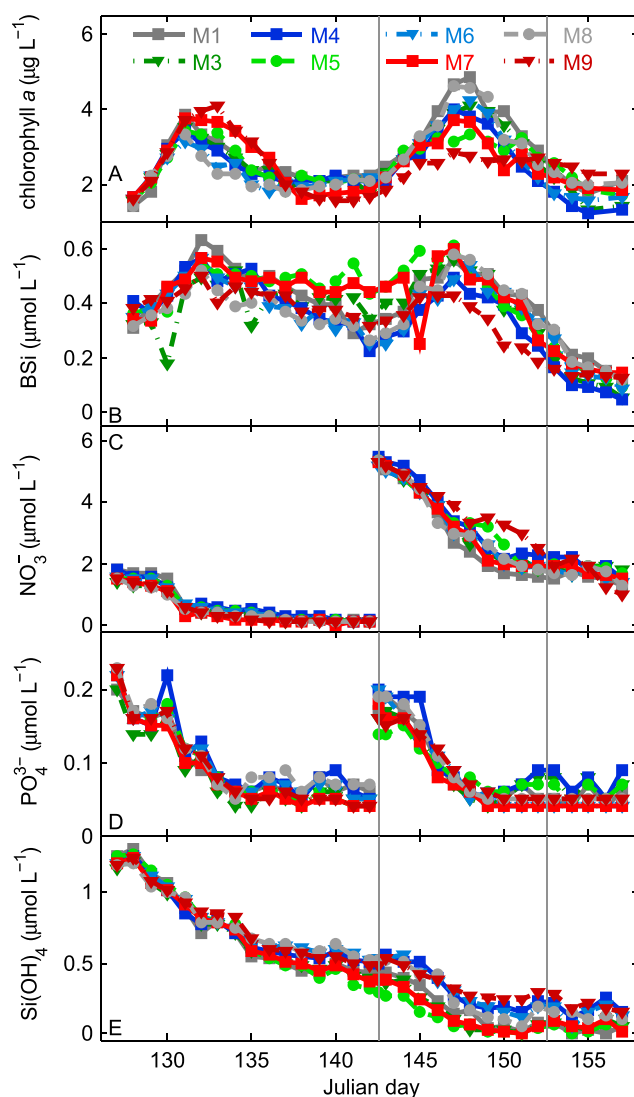


Figure 2. Temporal development of (A) chlorophyll *a*, (B) BSi, (C) NO_3^- , (D) PO_4^{3-} , and (E) Si(OH)_4 concentrations. Julian day 127 was the 7th of May. The vertical grey lines separate the three phases. NO_3^- and PO_4^{3-} were added on day 142.

3. Results

3.1. Plankton Community Structure

The mesocosms were closed during a postbloom period with rather low chlorophyll *a* and nutrient concentrations but relatively high numbers of mesozooplankton. After closing the mesocosms the water column was gently mixed by air bubbling in order to eliminate the salinity stratification. This procedure lifted nutrients from deeper mesocosm water layers to the brighter top, thereby stimulating photoautotroph growth in phase I (Figure 2A). The increase in chlorophyll *a* was paralleled by decreasing nutrient concentrations (Figures 2B–2D) and primarily due to growth of picoeukaryotes (0.2–2 µm), two groups of nanophytoplankton (NANO I (2–6 µm) and NANO II (6–20 µm)), and cryptophytes (2–20 µm; Figure 3). The two NANO groups were most likely the diatoms species *Arcocellulus* sp. and *Thalassiosira* sp. (R. Bermudez-Monsalve personal communications), which explains the increase in BSi (Figure 2E). Abundances of the coccolithophore *Emiliania huxleyi* (5–10 µm) and *Synechococcus* (0.6–1.6 µm) remained low at the beginning (Figure 3).

Copepod abundance was highest at the beginning of the experiment and ranged from ~12.9 (M1) to 15.3 (M7) individuals L^{-1} . Roughly half of the animals were nauplius larvae (between 44 and 58%), but they

2.7. Data Analysis

The change of organic matter ballasting, aggregate sinking velocities, size, $\rho_{\text{aggregate}}$ and $P_{\text{estimated}}$ over time were analyzed by means of time series analysis. Therefore, we averaged the daily response in the respective parameters over all eight mesocosms. Calculation of the daily average smoothed the data and facilitated the detection of trends.

Based on the trends observed in the averaged aggregate parameters we split the whole data set into three distinct phases: phase I = Julian days 128–142, phase II = Julian days 143–152, and phase III = Julian days 153–157. We subsequently tested for each time series parameter whether there is a significant trend (decrease or increase with time) in the respective phase by means of linear regression analysis using R (R Project for Statistical Computing). Results of these analyses are summarized in Table S1 in the supporting information. Please note that we stopped our analysis on Julian day 157, although the study lasted until day 163 because sinking velocity, the core parameter in the present study, was only measured until day 157.

Temporal developments in zooplankton abundance have not been analyzed with the time series approach because of low sampling frequency. The temporal development in phytoplankton abundance, chlorophyll *a*, and BSi was so obvious that a time series analysis was not necessary.

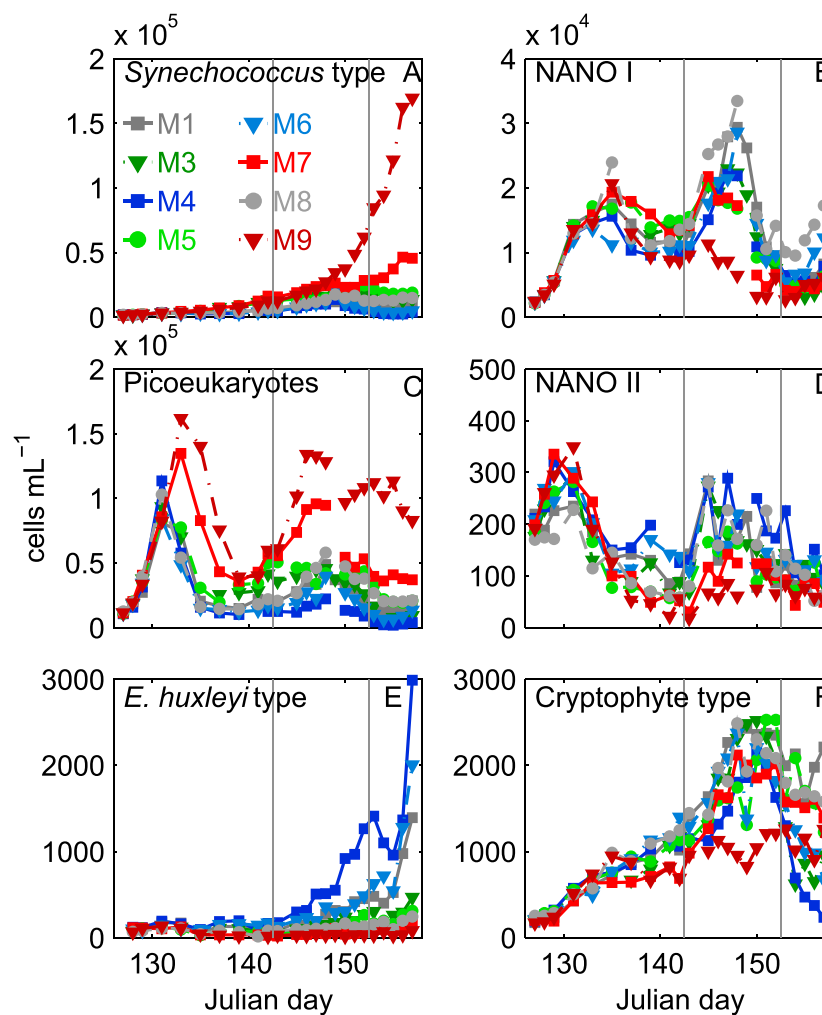


Figure 3. Temporal development of major phytoplankton functional types or genera. The vertical grey lines separate the three phases. NO_3^- and PO_4^{3-} were added on day 142.

developed to copepodites and adults during the first phytoplankton bloom (Figures 4A and 4C). Most of the copepods (generally more than 95%) belonged to the genera *Oithona*, *Temora*, *Pseudocalanus*, and *Calanus* throughout the entire experiment [Hildebrandt, 2014]. The loss of nauplii from the water column through sedimentation was low but higher at the beginning than at any other time of the experiment (Figure 4B). This contrasted the loss rates of copepodites and adults, which were generally on a higher level but lowest at the beginning (Figure 4D). Metazoan calcifiers such as pteropods, other gastropod larvae, and bivalve larvae (called mollusks in the following) were initially relatively abundant but quite constantly decreased during the entire experiment. Mollusk loss through sedimentation seemed to be higher at the beginning and toward the end of the experiment, although loss rates were difficult to quantify as there were large fluctuations between samplings (Figure 4F). Appendicularians, represented by the species *Oikopleura dioica*, were initially present in low numbers, and we observed an elevated loss through sedimentation at the beginning of the study (Figures 4G and 4H).

The initial phytoplankton bloom started to decline between Julian days 131 and 132 (Figure 2A) mainly due to a decreasing abundance of the PICO and NANO II groups (Figures 2C and 2D). The decline of NANO II was paralleled by decreasing BSi concentrations (Figure 2B), decreasing copepod abundances in the water column (Figures 4A and 4C), and increasing copepod loss rates through sedimentation (Figure 4D).

The addition of nutrients at the beginning of phase II (Figures 2B–2D) stimulated a second phytoplankton bloom (Figure 2A), which was primarily mediated by NANO I, NANO II, and cryptophytes, except for M9

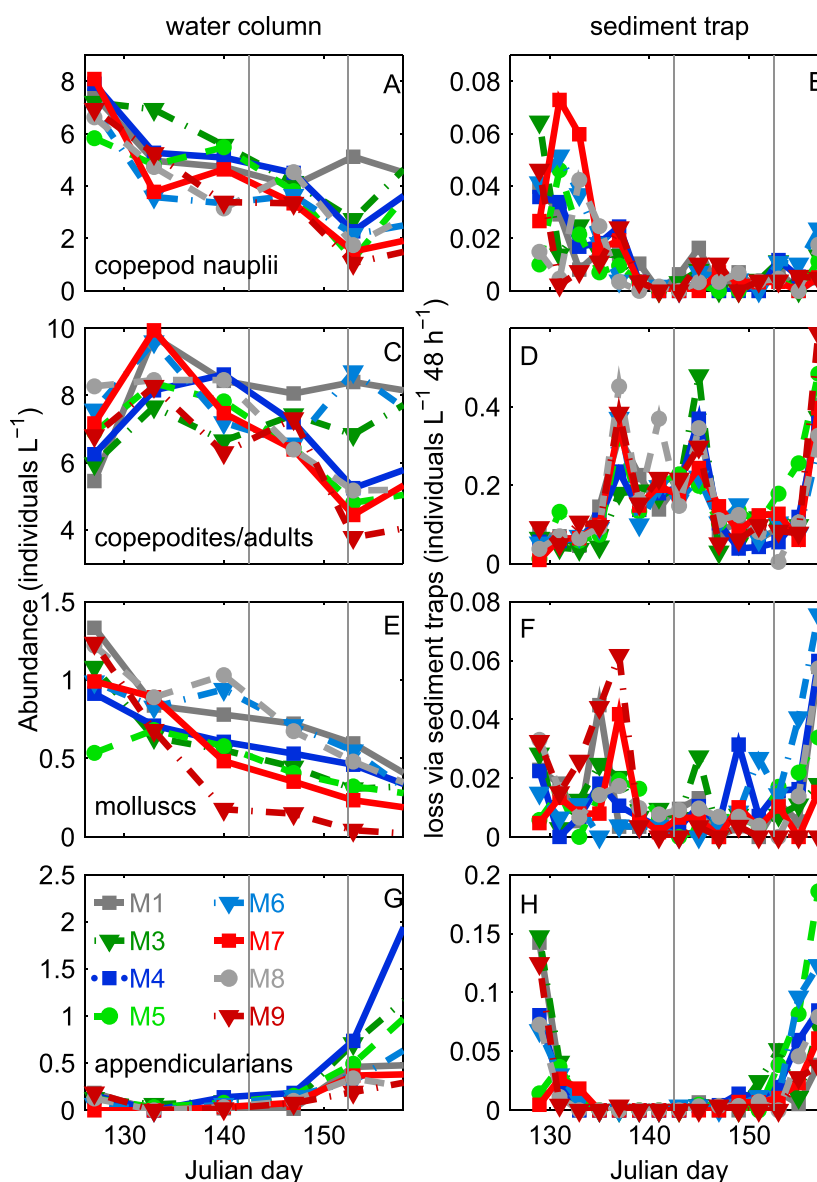


Figure 4. Mesozooplankton development. (A, C, E, G) Measured water column abundances of the major mesozooplankton types. (B, D, F, H) Loss rates of these types through sedimentation. Note that the last measurement of zooplankton abundance in the water column was on day 161, which was after sinking velocity measurements ended. The vertical grey lines separate the three phases. NO_3^- and PO_4^{3-} were added on day 142.

and to some extent also M7, where picoeukaryotes and *Synechococcus* were increasing instead (Figures 3B–3D and 3F). As in the first bloom, autotrophic growth was paralleled by buildup of biogenic silica (Figure 2B). Copepod abundances during the second bloom were comparable to those before the nutrient fertilization (Figures 4A and 4C). Their loss rates through sedimentation, however, decreased by about 50% and stayed at a low level until Julian day 155 (Figure 4D). Appendicularians were still low in abundance but started to increase in phase II until the end of the experiment (Figure 4G).

The second bloom started to decline around Julian day 148, but the decline rate varied among mesocosms. It was most pronounced in M1 and least pronounced in M9. Copepod and appendicularian abundance varied considerably among the mesocosms during the bloom decline. Their loss rates through sedimentation were generally low but increased when chlorophyll *a* concentrations reached baseline levels around Julian day 155.

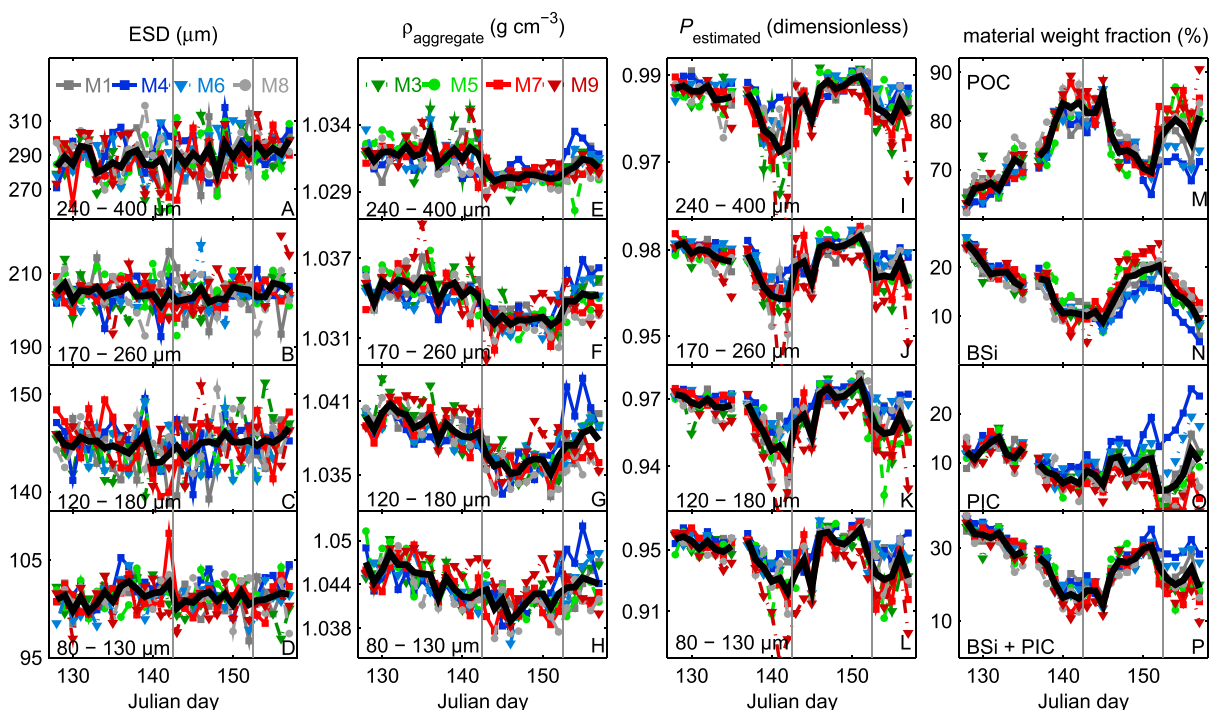


Figure 5. Temporal development of aggregate properties and ballasting. (A–D) ESD, (E–H) $\rho_{\text{aggregate}}$, and (I–L) $P_{\text{estimated}}$ of the aggregates within the four size classes. (M–P) Contribution of POC, BSi, and PIC to the total weight (excluding seawater) of the material collected in the sediment traps. Y axis labels are shown on top of each plot. The black line is the mean calculated as the daily average of all mesocosms. The vertical grey lines separate the three phases. NO_3^- and PO_4^{3-} were added on day 142.

Synechococcus and *E. huxleyi* strongly increased in abundances in some of the mesocosms toward the end of the experiment in phase III. *Synechococcus* was primarily blooming in M9 and M7 (up to 1.7 and 0.5×10^6 cells mL^{-1} , respectively; Figure 3A), while *E. huxleyi* thrived most noticeably in M4, M6, and M1 (up to 2800 , 1900 , and 1400 cells mL^{-1} , respectively; Figure 3E). The divergence of the plankton composition between mesocosms seen in Figures 3 and 4 is the result of different CO_2 concentrations. This will be discussed in detail in publications currently in preparation.

3.2. Aggregates Properties and Sinking Velocity

Average sizes of aggregates within the four size classes were 101 ($80\text{--}130\ \mu\text{m}$), 145 ($120\text{--}180\ \mu\text{m}$), 205 ($170\text{--}260\ \mu\text{m}$), and $289\ \mu\text{m}$ ($240\text{--}400\ \mu\text{m}$). Size was comparatively stable and showed little change over time (Figures 5A–5D), although it must be kept in mind that the particle size distribution in the settling column potentially deviated from the size distribution inside the mesocosms due to sample preparation [Boxhammer *et al.*, 2016] (see also section 2.3).

The $\rho_{\text{aggregate}}$ of the four size classes averaged over the whole experiment decreased with aggregate size from 1.044 ($80\text{--}130\ \mu\text{m}$), over 1.038 ($120\text{--}180\ \mu\text{m}$), 1.034 ($170\text{--}260\ \mu\text{m}$), to $1.031\ \text{g cm}^{-3}$ ($240\text{--}400\ \mu\text{m}$). The $\rho_{\text{aggregate}}$ decrease with size (Figure S2A) was due to the modular or fractal organization of aggregates [Allredge and Gotschalk, 1988; Burd and Jackson, 2009]. Development of $\rho_{\text{aggregate}}$ over time was comparable among all size classes (Figures 5E–5H). Phase I was characterized by consistently high $\rho_{\text{aggregate}}$ in the larger two size classes and initially high but significantly decreasing $\rho_{\text{aggregate}}$ in the two smaller ones (Figures 5E–5H and Table S1). During phase II $\rho_{\text{aggregate}}$ suddenly dropped (larger two size classes) or continued dropping for 3 days (smaller two size classes) before reaching a baseline value, at which they remained until the end of the second phase. The last phase was characterized by a treatment-specific development in $\rho_{\text{aggregate}}$ with those mesocosms with higher abundances of the coccolithophore *E. huxleyi* having higher values.

In the different size classes, $P_{\text{estimated}}$ averaged over the whole experiment was 0.946 ($80\text{--}130\ \mu\text{m}$), 0.963 ($120\text{--}180\ \mu\text{m}$), 0.976 ($170\text{--}260\ \mu\text{m}$), and 0.984 ($240\text{--}400\ \mu\text{m}$), which is in very good agreement with the results

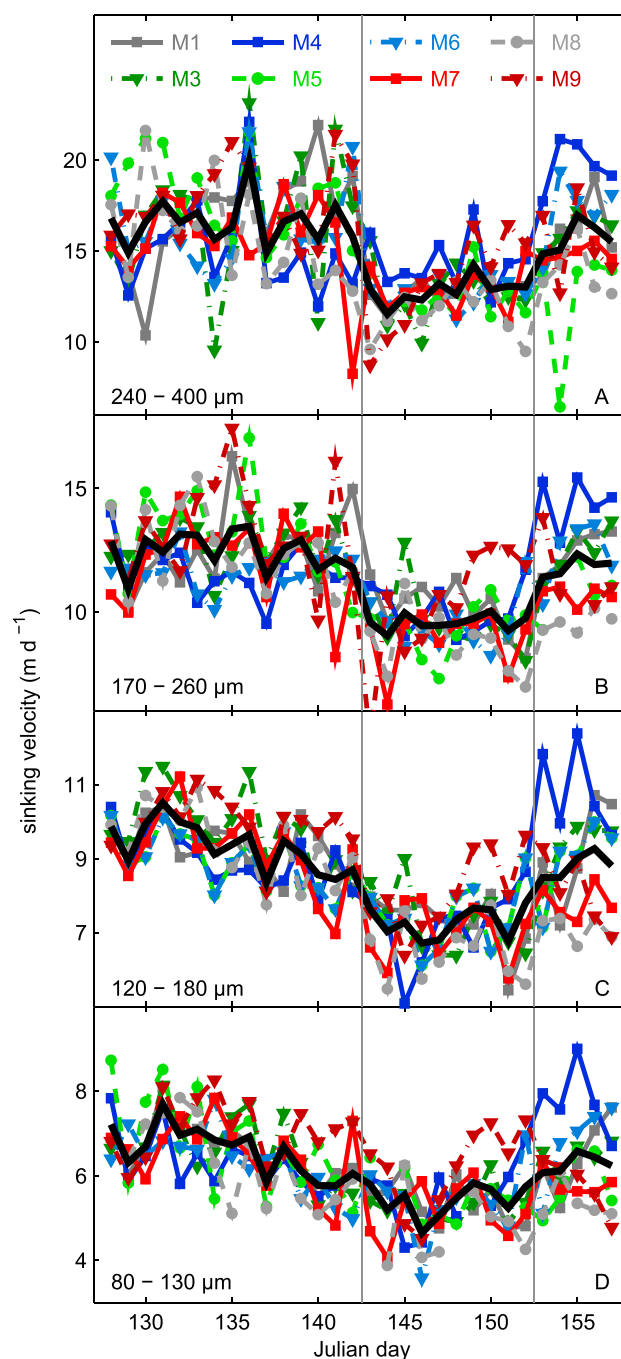


Figure 6. (A–D) Measured sinking velocities of the four size classes (with Figure 6D being the smallest). The black line is the mean sinking velocity calculated as the daily average of all mesocosms. The vertical grey lines separate the three phases. NO_3^- and PO_4^{3-} were added on day 142.

3.3. Ballasting of Sediment Trap Material

At the beginning of the experiment roughly 65% of the total sediment material weight were made up by organic matter, while silica and CaCO_3 contributed 25 and 10%, respectively (Figures 5M–5P). The fraction of silica and CaCO_3 decreased steadily until day 140 to ~12 and 7%, respectively. The continuous reduction of silica ballasting during this period was paralleled by the decline of diatoms and BSi in the water column (Figures 2B and 5N). The reduction of CaCO_3 contribution in phase I was not reflected in a decrease of E .

from earlier studies [Allredge and Gotschalk, 1988; Lam and Bishop, 2007; Engel et al., 2009]. The increase of $P_{\text{estimated}}$ with aggregate size is a commonly observed feature and due to the fractal nature of aggregates [Allredge and Gotschalk, 1988; Burd and Jackson, 2009]. Development of $P_{\text{estimated}}$ over time was similar among the four size classes. It decreased significantly throughout phase I (Table S1) but developed some treatment-specific differences toward the end of this phase (Figures 5I–5L). Differences were most pronounced in M9, which generated aggregates with lower $P_{\text{estimated}}$. The treatment-specific differences in $P_{\text{estimated}}$ were still present at the onset of phase II. However, $P_{\text{estimated}}$ was starting to increase again in all mesocosms and reached a second peak shortly after the second peak in chlorophyll *a* near the end of phase II (compare Figures 2A and 5I–5L). $P_{\text{estimated}}$ decreased during the last 2 days of phase II, but the decline was treatment specific. It was again most pronounced in M9 (Figures 5I–5L).

Aggregate sinking velocities averaged over the whole experiment were 6.1 (80–130 μm), 8.6 (120–180 μm), 11.4 (170–260 μm), and 15.2 (240–400 μm) m d^{-1} , respectively, and increased with aggregate size (Figure S2B). Changes in sinking velocity over time are similar among the four size classes (Figure 6) reflected in the linear correlation between sinking velocities of different size classes (Figure S2C). Its temporal development mirrored changes in $\rho_{\text{aggregate}}$ (see above and compare Figures 6 and 5E–5H). Thus, all relevant changes in aggregate sinking velocity measured in the settling columns were caused by changes in their density properties.

huxleyi cell abundance (Figures 3E and 5O) but may instead either be attributable to (1) decreasing coccolith production rate at stable *E. huxleyi* population size, (2) the dwindling presence of calcifying mollusk larvae (Figure 4E), or (3) to a declining abundance of bacteria-derived CaCO_3 precipitates [Heldal et al., 2012] (see also section 4.1.1).

Silica contribution to total density started to increase again on day 146, which was 4 days after the nutrient addition (Figure 5N). The increased share of silica material in the sediment trap of 15–25% shortly after the peak of the second bloom (Julian day 150) coincides with a decline of water column BSi as well as NANO I and NANO II abundances (Figures 2B, 3B, and 3D). Silica contribution decreased linearly after day 150 reflecting the decrease of BSi in the water column. Its contribution was 5–13% at the end of the experiment.

CaCO_3 contribution to total density generally scaled positively with *E. huxleyi* abundance for the time after the nutrient addition until the end of the experiment. Highest *E. huxleyi* abundance in M4 translated to 28% CaCO_3 contribution to weight fraction of sediment trap material at the end of the experiment. In contrast, CaCO_3 was not contributing at all to the material weight in M9 during this phase (Figure 5O), where *E. huxleyi* appeared in very low abundances (Figure 3E).

3.4. Relevance of Changes in Sinking Velocity for Particulate Matter Transfer Efficiency

Aggregate sinking velocities changed considerably in the course of the experiment in response to the plankton community succession (Figure 6). We formulated the one-dimensional carbon flux model (equation (9)) in order to assess whether changes within this scale could be relevant for particulate matter sequestration. Results of this sensitivity analysis are shown in Figures S3A and S3B. The pattern of particle remineralization resembled a Martin curve, irrespective of the modeled sinking velocities. Flux attenuation was negatively correlated with sinking velocities (Figure S3A). Transfer efficiency between 100 and 1000 m depth increased by about 0.25% per 1% increase in modeled sinking velocity (Figure S3B).

4. Discussion

Linking plankton community structure with measurement of export-relevant parameters by means of in situ mesocosm studies has recently been identified as a research priority [Sanders et al., 2014]. We enclosed a natural plankton community in a Norwegian fjord and were able to follow its development for more than a month under close to natural conditions (see video by Boxhammer et al. [2015] to get an impression on the plankton community). This experiment is the first in a series of several (Swedish coast, 2013; Coast off the Canary islands, 2014; Norwegian coast, 2015), where sinking velocity measurements with high temporal resolution [Bach et al., 2012a] were linked with plankton community structure within the mesocosms. We will therefore not only address the major hypothesis and outcomes of the study (section 4.1) but also discuss limitations and illustrate potential improvements of the mesocosm approach (section 4.2).

4.1. Influence of the Plankton Community Structure on Aggregate Properties and Sinking Velocities

4.1.1. Was There a Transition from Ballast to Packaging-Dominated Control on Sinking Velocity?

The first phytoplankton bloom was characterized by high BSi concentrations in the water column and a large copepod population developing from nauplii into adults. Aggregates sank relatively fast during this period, which appears connected to a large CaCO_3 and BSi ballast loading (Figure 5P) rather than low $P_{\text{estimated}}$ (Figures 5I–5L).

Potential CaCO_3 -forming organisms present in the mesocosms at this time comprised *E. huxleyi* (Figure 3E), metazoan calcifiers (Figures 4E and 4F), and bacteria which can contribute up to $\sim 0.3 \mu\text{mol kg}^{-1}$ of inorganic CaCO_3 as particles (1–100 μm) in Raunefjord [Heldal et al., 2012] through the release of polyamines [Yasumoto et al., 2014]. We estimated CaCO_3 supply by *E. huxleyi* based on the assumptions that each cell contributed a total of 2 pmol CaCO_3 (1 pmol within the coccosphere plus 1 pmol as detached coccoliths [Balch et al., 1993]). The presence of 52–185 cells mL^{-1} during the first 7 days (Figure 3E) would result in a water column coccolithCaCO_3 standing stock of 0.1–0.37 $\mu\text{mol L}^{-1}$, whereas the corresponding CaCO_3 accumulation rate in the sediment traps ranged from 0.012 to 0.052 $\mu\text{mol L}^{-1} \text{d}^{-1}$ during this period (CaCO_3 sedimentation data not shown). We estimated that 8–37% loss of the coccolithCaCO_3 standing stock per day could fully account for the bulk CaCO_3 recovered from the sediment traps during the first 7 days. Such a loss rate could have been easily compensated by new coccolith production by the *E. huxleyi* population [Bach et al., 2012b] inside the

mesocosms. Thus, CaCO₃ ballast recovered from the sediment traps during the first 7 days could have potentially been supplied to a large extent by *E. huxleyi*. The relevance of other CaCO₃ sources remains unclear, but since, for example, metazoan shells were sparse and have a lower carrying capacity for organic matter, they may not have been particularly efficient ballast materials [Schmidt *et al.*, 2014].

Opal ballast particles were generated by diatoms (mainly *Arcocellulus* sp. and *Thalassiosira* sp.), which were the only silicifiers present in noticeable quantity by this time. Both diatom frustules and *E. huxleyi* coccoliths are small (~3–15 μm), which allows them to be more homogeneously incorporated into an organic aggregate matrix and serve as efficient ballast particles [Schmidt *et al.*, 2014]. Hence, we assume that relatively fast sinking during the first bloom was primarily due to opal ballasting by diatoms and presumably CaCO₃ ballasting by *E. huxleyi*.

The contribution of BSi and CaCO₃ to the total weight of sediment trap material was rapidly decreasing from ~27% (day 137) to 16% (day 140) after the first bloom. Sinking velocities, however, were not noticeably affected by the sudden decline in ballasting (Figure 6). The absence of a clear reduction of sinking velocities can be explained by declining $P_{\text{estimated}}$ (i.e., increasing aggregate compactness), which compensated for the reduction of BSi and PIC ballasting during this time (Figures 5I–5L). Interestingly, the estimated shift toward less porous aggregates happened when chlorophyll *a* reached baseline levels and NO₃[−] and PO₄^{3−} were close to (NO₃[−]) or within (PO₄^{3−}) the detection limits (Figures 2A–2C). Therefore, we speculate that the decrease in $P_{\text{estimated}}$ could have been caused by a transition in the food web from a diatom-dominated food web fueled by upwelled nutrients (new production) toward one, which was increasingly dependent on remineralized nutrients (regenerative production). Presumably, the shift toward regenerative production may have intensified recycling and led to a more thorough removal of fresh and fluffy components from the POC standing stock. This hypothesis is supported by observations of higher POC and PON contents in diatom-derived marine snow compared to aggregates containing more decomposed components [Alldredge, 1998]. The preferential removal of fluffy components would lead to an accumulation of more densely packed material in the sinking material [Lam *et al.*, 2011]. Additionally, this repackaging may have been further amplified by copepods feeding on sediment trap material since we counted increasing numbers of living copepods in the sediment trap samples at the point when chlorophyll *a* concentrations consolidated at a temporal minimum after the first bloom (compare Figures 2A and 4D). Organic matter became sparse in the water column at this time so that more and more copepods may have detected the sediment trap as an additional food source [Lampitt *et al.*, 1993].

4.1.2. Sinking Velocity Control Through Aggregate Porosity? The Potential Role of Plankton Community Structure

The addition of nitrate and phosphate to all mesocosms (Figures 2B and 2C) on day 142 initiated a second phytoplankton bloom. Diatoms were a prominent component in this second bloom (Figure 2B) as there was still dissolved silicate left in the system (~0.5 μmol L^{−1} on day 142). The loss rate of copepods through sedimentation declined during bloom buildup, suggesting that the animals were attracted by the fresh food growing in the water column and relied to a lesser extent on debris collected in the sediment trap.

Sinking velocities responded to these water column processes with a profound decline and reached experiment minima briefly after nutrient addition (Figure 6). To our surprise, these lowest velocities were sustained throughout the entire diatom bloom between days 142 and 152 even though increasing amounts of BSi ballast were collected in the sediment traps with a ballasting potential close to that observed during the first bloom (Figure 5N). The absence of a positive BSi ballast effect on sinking velocities during the diatom bloom could have three different reasons. First, BSi ballast was not integrated into the aggregate matrix. This is unlikely, however, considering that much of it originates from small diatoms (section 3.1), which should have a high potential to attach to organic matter due to their relatively high scavenging potential [Burd and Jackson, 2009; Schmidt *et al.*, 2014]. Second, the dominant diatoms coagulated within aggregates actively downregulated their excess density in order to remain at higher light intensities during nutrient-fertilized growth as seen for large chain-forming species [Moore and Villareal, 1996]. This explanation is also rather unlikely, since large chains were hardly present in our study and decelerated sinking under nutrient-repleted conditions is a species-dependent, not a universal feature of diatoms [Bienfang *et al.*, 1982]. Third, perhaps most likely seems to be that high $P_{\text{estimated}}$ (Figures 5I–5L) decelerated sinking velocity and thus overcompensated the positive influence of mineral ballast during that time. This conclusion is also supported by

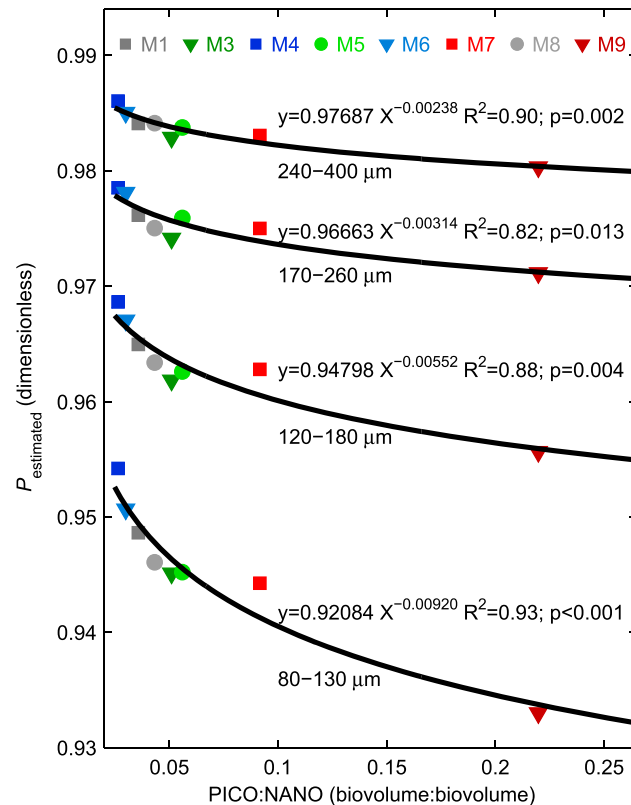


Figure 7. Influence of plankton community structure on $P_{\text{estimated}}$. Estimated cell diameters used for biovolume calculations (assuming spherical shape) were *Synechococcus* = 1 μm, picoeukaryotes = 1 μm, NANO I group = 3 μm, NANO II group = 10 μm, *E. huxleyi* = 6 μm, and cryptophytes = 7 μm. Biovolume was subsequently calculated by multiplication of flow cytometry counts (Figure 3) with species-specific biovolumes. The sum of biovolume of species smaller than 2 μm (*Synechococcus* and picoeukaryotes) divided by the sum of biovolume provided by species larger than 2 μm (NANO I, NANO II, *E. huxleyi*, and cryptophytes) is the PICO:NANO ratio. Shown here is the PICO:NANO ratio and $P_{\text{estimated}}$ averaged over the whole experiment with one line for each of the four aggregate size classes.

our daily inspections of the sediment trap samples, where we noted that the collected material looked like a fluffy mush rather than a consortium of individual particles.

Comparing the succession of $P_{\text{estimated}}$ during bloom one (phase I) with that of bloom two (phase II + phase III) reveals a remarkably similar pattern. $P_{\text{estimated}}$ was rather high in both blooms as long as the system was in a “new production state,” where biomass buildup is fueled by upwelled or added inorganic nutrients. $P_{\text{estimated}}$ decreased, however, when switching back to a “regenerative state” under low inorganic nutrient concentrations in the aftermath of a bloom (compare Figures 2B and 2C and Figures 5I–5L). These observations are in line with a growing body of literature that export of aggregates generated during the typical diatom spring bloom is relatively inefficient due to their high porosity (i.e., low packaging) [Francois et al., 2002; Lam and Bishop, 2007; Lam et al., 2011; Puigcorb  et al., 2015].

To further explore mechanisms controlling packaging we not only looked at the temporal development of $P_{\text{estimated}}$ but also had a closer look on the differences among mesocosms. Differences were generally small and the overall trend was similar, but we noticed that $P_{\text{estimated}}$ tended to be lower in those mesocosms, which harbored higher numbers of picophytoplankton (e.g., M5, M7, and M9; Figures 3A and 3C). In order to test this observation, we first calculated the biovolume of all phytoplankton groups (Figure 9), then calculated the ratio of groups smaller 2 μm (PICO) to groups larger 2 μm in diameter (NANO), and thereafter correlated the average PICO/NANO ratio with the average $P_{\text{estimated}}$ (Figure 7). We found a negative correlation between the PICO/NANO ratio and $P_{\text{estimated}}$ in all four aggregate size classes (Figure 7), which suggests that plankton communities with abundant picophytoplankton tend to generate more tightly packed aggregates than communities where a higher fraction of the biomass is accumulated in larger species. This observation is

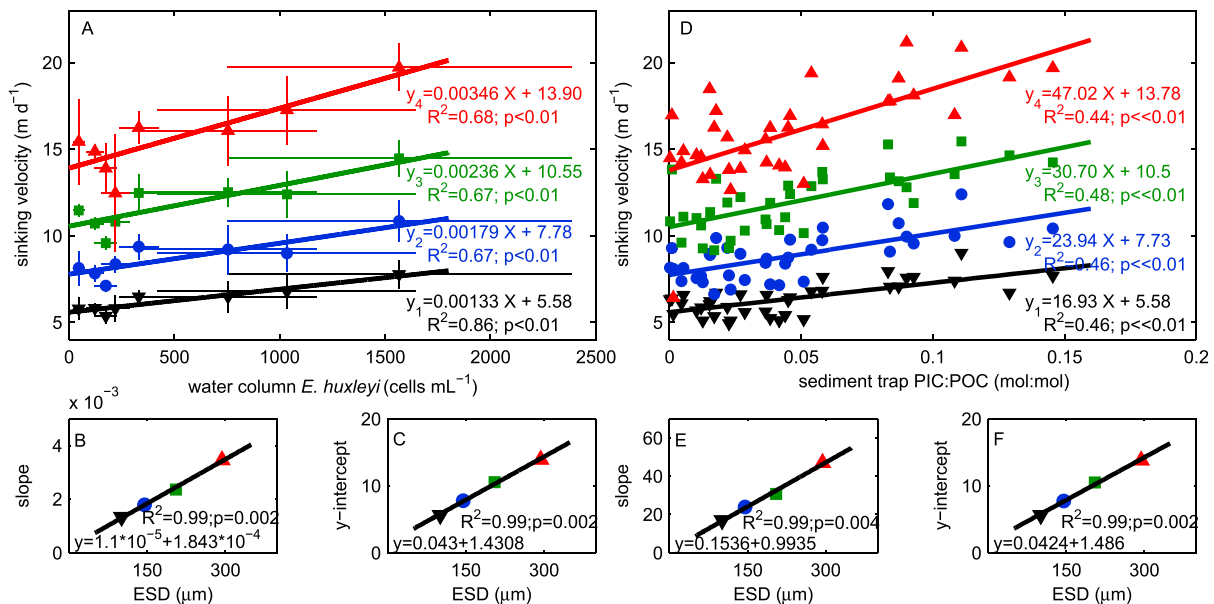


Figure 8. Influence of the *E. huxleyi* blooms on sinking velocities during phase III. (A) Sinking velocities of the four size classes (black triangles: 80–130 μm; blue dots: 120–180 μm; green squares: 170–260 μm; red pyramids: 240–400 μm) as a function of water column *E. huxleyi* abundance. Each data point represents the phase III average of one mesocosm with error bars being standard deviations. Note that we calculated phase III averages (instead of using daily measurements during phase III) as we are unable to tell with what temporal delay *E. huxleyi* cells arrive in the sediment traps. (B) Correlations between slopes and average ESD or (C) y intercepts and average ESD of the regressions calculated in Figure 8A. (D–F) The same results as in Figures 8A–8C, but in this case, sinking velocities are a function of PIC:POC ratio measured in sediment trap material. Note that data from individual days during phase III could be used in Figure 8D in contrast to Figure 8A because measurements of PIC:POC and sinking velocities were done with material collected on the same day.

mechanistically reasonable because small aggregate components allow relatively little interstitial space between them [Burd and Jackson, 2009]. Furthermore, PICO-dominated communities usually prevail in regenerative systems, where particles potentially undergo a relatively large degree of biotic reprocessing and therefore a continuous compression [Lam et al., 2011]. With respect to particle matter export, low $P_{estimated}$ aggregates formed in a high PICO/NANO regime would promote transfer efficiencies as they probably sink faster than fluffy aggregates. Thus, the negative correlation between PICO/NANO and $P_{estimated}$ (Figure 7) observed in our study may help to explain the numerous observations that low productivity regimes tend to generate particles with high transfer efficiencies [Francois et al., 2002; Lam and Bishop, 2007; Lomas et al., 2010; Lam et al., 2011; Henson et al., 2012a, 2012b; Maiti et al., 2013; Cavan et al., 2015; Puigcorb  et al., 2015].

4.1.3. The Potential for Sinking Velocity Acceleration by *E. Huxleyi*-Derived CaCO₃ Ballast

Phase III was characterized by decreasing chlorophyll *a* and BSi concentrations as well as treatment-specific developments within major phytoplankton and zooplankton types (Figures 3 and 4). The differential developments among mesocosms were reflected in particle sinking velocities, where those mesocosms which harbored significant *E. huxleyi* blooms generated aggregates with some of the highest sinking velocities measured during the entire study, while aggregate sinking velocities remained at a low level in mesocosms where *E. huxleyi* growth was muted (Figures 3 and 6).

The acceleration of sinking velocities in phase III was most likely due to CaCO₃ ballast provided by *E. huxleyi* (Figure 8) and rather not caused by tight packaging because $P_{estimated}$ was higher in those treatments with high CaCO₃ availability (compare Figures 5I–5L with 5O). We used the positive correlations between particle sinking velocity and *E. huxleyi* abundance (Figure 8A) or sediment material PIC:POC ratio during phase III (Figure 8D) to estimate the influence of *E. huxleyi*-dependent acceleration of particle sinking velocity on transfer efficiency with the one-dimensional particle flux model (equation (9)) derived in section 2.6. Therefore, slopes and the y intercepts of the four sinking velocities versus PIC:POC or cell abundance correlations (see Figures 8A and 8D) were plotted against average ESD of the respective size class. Slopes and y intercepts of the four correlations increased with average aggregate size (Figures 8B, 8C, 8E, and 8F), which is expected according to Stokes' law. With the slopes versus ESD (Figures 8B and 8E) and y intercepts versus ESD

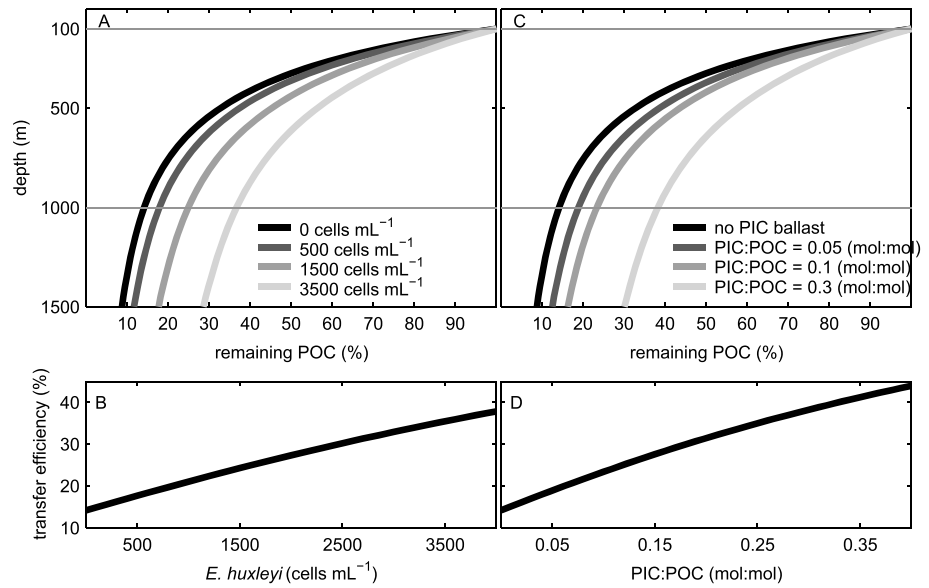


Figure 9. Influence of the *E. huxleyi* blooms on transfer efficiencies during phase III calculated with the one-dimensional carbon flux model (section 4.1.3). (A) Flux attenuation as a function of different *E. huxleyi*-dependent sinking velocity parameterizations (section 4.1.3; Figure 8a). The upper and lower horizontal grey lines indicate the bottom of the euphotic zone and sequestration depth, respectively. (B) Increase of transfer efficiency with *E. huxleyi* abundance in the euphotic zone. (C and D) The same results as in Figures 9A and 9B, but in this case, sinking velocities are a function of PIC:POC ratio measured in sediment trap material (section 4.1.3; Figure 8D).

(Figures 8C and 8F) correlations, we were able to parameterize the dependency of sinking velocities on either sediment material PIC:POC ratio or water column *E. huxleyi* abundance (N_{ehux}) as

$$\text{Sinkingvelocity}_{\text{PIC:POC}} = \text{slope}_{\text{PIC:POC}} \times \text{PIC : POC} + \text{intercept}_{\text{PIC:POC}} \quad (11)$$

and

$$\text{Sinkingvelocity}_{ehux} = \text{slope}_{ehux} \times N_{ehux} + \text{intercept}_{ehux} \quad (12)$$

where $\text{slope}_{\text{PIC:POC}}$ and slope_{ehux} as well as $\text{intercept}_{\text{PIC:POC}}$ and intercept_{ehux} were taken from regressions shown in Figures 8B, 8C, 8E, and 8F. The *E. huxleyi*- or PIC:POC-dependent acceleration of sinking velocities can subsequently be included in the export model (equation (9)) by multiplying the sinking velocity_{model} term with the $ehux_{\text{factor}}$ or the $\text{PIC:POC}_{\text{factor}}$, defined as

$$ehux_{\text{factor}} = \frac{\text{slope}_{ehux} \times N_{ehux} + \text{intercept}_{ehux}}{\text{intercept}_{ehux}} \quad (13)$$

and

$$\text{PIC : POC}_{\text{factor}} = \frac{\text{slope}_{\text{PIC:POC}} \times \text{PIC : POC} + \text{intercept}_{\text{PIC:POC}}}{\text{intercept}_{\text{PIC:POC}}} \quad (14)$$

Hence, U_{model} in equation (9) increases about a certain percentage throughout the entire water column, similar as has been simulated in the sensitivity analysis conducted in section 3.4. This time, however, sinking velocity is not increased by an arbitrary factor but scales with *E. huxleyi* cell concentrations in the euphotic zone or the PIC:POC ratio of the sinking aggregates.

Sinking velocity acceleration was already profound under relatively low *E. huxleyi* abundances or PIC:POC ratios (Figures 8A and 8D), which also considerably increased transfer efficiencies (Figure 9). For example, we estimated an acceleration of almost 40% for an increase in *E. huxleyi* abundance from 0 to 1500 cells mL⁻¹ or a PIC:POC increase of ~0.1 (Figures 8A and 8D). Such a ballast-mediated increase in sinking velocity could elevate transfer efficiencies from 14 to 24% (Figure 9). The key question now is: Are *E. huxleyi* cell densities of 1500 cells mL⁻¹ and the corresponding increase in PIC:POC exceptional or common in the

oceans? Abundances of up to 1000 [Poulton *et al.*, 2013], 1500 [Balch *et al.*, 1991], and even 20,000 coccospheres mL^{-1} [Holligan *et al.*, 1993] were counted during bloom seasons on the Patagonian Shelf, the Gulf of Maine, and south of Iceland (63°N, 20°W), respectively. Kopelevich *et al.* [2014] calculated that *E. huxleyi* often reaches abundances of 3000 cells mL^{-1} or even more during the typical coccolithophore summer bloom in the Black Sea. An estimated 3 mmol PIC m^{-3} contributed by 1500 cells mL^{-1} (assuming 2 pmol PIC cell⁻¹ [Balch *et al.*, 1993]) also compares reasonably well with data from the satellite studies by Moore *et al.* [2012] and Hopkins *et al.* [2015], who found coccolithophore PIC of 1–10 mmol m^{-3} to be common on shelves and many regions of the open ocean during bloom season. Based on these assessments on *E. huxleyi* abundance we conclude that *E. huxleyi*-associated particle sinking velocity accelerations of ~40% or even more are perhaps not unusual. Thus, the regional and/or seasonal occurrence of *E. huxleyi* blooms may mark events of highly efficient sequestration pulses.

4.2. Sinking Velocity Measurements of Mesocosm Sediment Trap Material: Uncertainties, Limitations, and Future Directions

4.2.1. Influence of Lithogenic Ballast Materials

Some of the highest sinking velocities of the entire experiment were measured during the first days (Figure 6). As lithogenic material has not been quantified in this study, it cannot be ruled out that the initially fast sinking rates are due to lithogenic ballast minerals enclosed while lowering the mesocosm bags at the beginning of the experiment. However, mesocosm bags were closed 4 days before the first sinking velocity measurement and the sediment traps were emptied on a daily basis until then. Artificial seeding of mesocosms with Saharan dust particles (99% <1 μm in size) showed that fastest sinking dust particles are transferred to 9.5 m within hours [Bressac *et al.*, 2012]. Smaller particles remained longer in the water column but also declined considerably within 2 days [Bressac *et al.*, 2012]. Thus, if lithogenic ballast particles were present in relevant quantities at the beginning of our experiment, then most of it should have sunk out of the water column before the first sinking velocity measurement.

The Icelandic volcano Grímsvötn erupted in the course of the experiment on 21 May. Part of the Grímsvötn ash plume passed the Raunefjord area during the night from 24 to 25 May (days 144–145) with ash concentrations ranging from 200 to 4000 $\mu\text{g m}^{-3}$ air and ash particle sizes between ~1 μm and 50 μm [Tesche *et al.*, 2012; Lieke *et al.*, 2013]. Sinking velocities, however, remained low after the ash passage (Figure 5) for at least another 4 days, which is too long considering that particles within this size class should have arrived much earlier in the sediment trap. Furthermore, the acceleration of sinking velocity 4 days after the ash passage was inconsistent among mesocosms, which is in contrary to expectations in case of such a dust-seeding event. Thus, it is concluded that dust from the Grímsvötn eruption was unlikely to have a significant ballast effect on mesocosm aggregates, either because ash concentrations were too low or because they were insufficiently collected by the mesocosms.

Based on these two lines of evidence we conclude that lithogenic ballast materials did not play a crucial role in the present study. Nevertheless, it is advisable to quantify their influence in mesocosm experiments on particle export because they may play an important role in other settings, where dust influx is more likely.

4.2.2. Sampling-Associated Limitations and Potential Improvements

Prior to sinking velocity determination, aggregates had to be pumped from the sediment trap to the surface, carried to land in a bottle, and prepared for the measurements (see section 2.3). This procedure provoked aggregate fragmentation and reassembly, which potentially influenced aggregate porosity and density and likely influenced aggregate size. Potential effects on porosity and density should be relatively constant over time and thus of minor consequence on the trends observed in this study. The likely modification of the aggregate size structure prevented us from investigating if changes in the plankton community composition could influence aggregate sinking velocity through changes in aggregate size structure.

Our method to measure sinking velocities (as set up in this study) is restricted to particles from 80 to 400 μm in ESD [Bach *et al.*, 2012a]. Although particles of that size are responsible for a large fraction of organic matter export to depth, we missed the important influence of particles outside that range [Clegg and Whitfield, 1990; Ebersbach and Trull, 2008; Durkin *et al.*, 2015]. In our study it is likely, however, that sinking velocities of aggregates >400 μm would have shown a similar response to changing plankton community structure as the ones below this threshold as long as they are composed of smaller aggregate building blocks. The same principle should apply for aggregates <80 μm but only until they become so small that they reach the size of

individual components (e.g., single-diatom cells), where their specific chemical composition no longer averages out in the aggregate matrix. The good correlation between sinking velocities of aggregates from different size classes (Figure S2C) supports the notion that temporal trends observed between 80 and 400 μm could to some extent also be found outside this size range.

The focus on rather small aggregates in this study (80–400 μm) explains comparatively slow sinking rates, ranging from an average of 6 m d^{-1} in the smallest size class (80–120 μm) to 15 m d^{-1} in the largest one (240–400 μm). Extrapolation based on the size versus velocity correlation given in Figure S2B projects settling rates of about 200 m d^{-1} for 4 mm large aggregates. This aligns well with in situ measurements yielding 1.3–287 m d^{-1} at a particle size of 0.2–20 mm [Diercks and Asper, 1997; PilskaIn et al., 1998; Nowald et al., 2009] and in situ sensor estimates yielding 10–200 m d^{-1} at a size of 0.07–6 mm [Mcdonnell and Buesseler, 2010; Jackson et al., 2015]. They tend to be somewhat lower, however, than sinking velocities calculated from sediment trap deployments with either the “benchmark” method (average of 70 to 450 m d^{-1} [Berelson, 2002; Fischer and Karakaş, 2009; Xue and Armstrong, 2009]) or specialized settling velocity sediment traps (ranging from 1 to 2000 m d^{-1} [Armstrong et al., 2009; Alonso-González et al., 2010]). Potential explanations for discrepancies between direct measurements and sediment trap-derived estimates could be poor trapping efficiency of slow sinking particles [Baker et al., 1988], leading to their underrepresentation in the sediment trap sample or remineralization of slow sinking particles before reaching the usually quite deeply deployed sediment traps.

Aggregate remineralization is the other factor (next to sinking velocity) controlling the attenuation of POM flux with depth (equation (9)). In the present study we neglected remineralization rate but we assume that changes in this parameter are opposite to the changes in sinking velocity. For example, tightly packed aggregates will sink faster than similar-sized fluffy aggregates but their remineralization will probably be slower because less porous particles have a reduced surface to volume ratio. Likewise, ballast-mediated acceleration of sinking velocities can be accompanied by reduced remineralization rates in case the ballast encloses and physically protects the organic matter [Francois et al., 2002]. Thus, we speculate that the calculated trends in transfer efficiencies would be amplified rather than buffered by changes in remineralization rates.

4.2.3. Restriction to Surface Ocean Processes: The Need for “Meso-Pelagi-Cosms”

The water column enclosed in the mesocosms was 25 m deep. Accordingly, the time from particle formation in the water column to collection in the sediment trap is relatively short and particles experienced little modifications after production. Our analysis is therefore restricted to processes taking place in the epipelagic but leaves postproduction particle modifications within the mesopelagic realm unconsidered. Thus, sinking velocities reported here should be seen as “entry speed” of aggregates at the beginning of their descent into the deep.

This limitation could be solved by designing significantly longer mesocosm bags than the ones used here—ideally ones which reach hundreds of meters deep into the mesopelagic. These Meso-pelagi-cosms would fully exclude advection and therefore enable us to understand and precisely quantify organic matter fluxes into the deep, how they depend on the plankton community in the euphotic zone, and how they are attenuated below the euphotic zone. Although construction and successful deployment of such Meso-pelagi-cosms are technically challenging, it may be worth aiming for such an approach in the future.

5. Conclusions

In this study we have investigated the influence of community structure on aggregate sinking velocity. We conclude that plankton communities influence sinking velocities primarily by providing ballast minerals and modifying aggregate porosity, although it must be kept in mind that the porosity estimate in this study ($P_{\text{estimated}}$) is a highly derived parameter and therefore associated with uncertainties (sections 2.5 and 4.2.2). Our observations point toward the following: (1) Ballast availability was relatively high when phytoplankton blooms were fueled by inorganic nutrients and dominated by diatoms. Yet sinking velocities of aggregates generated during these bloom were not necessarily accelerated by ballast. This could be related to the relatively high porosity of aggregates produced when the plankton community is in a new production state. (2) $P_{\text{estimated}}$ tended to decrease in postbloom periods, which we hypothesize to be caused by a shift from new to regenerated production. (3) $P_{\text{estimated}}$ averaged over the entire study period was lower in those mesocosms, where picophytoplankton contributed a larger fraction to the autotrophic biovolume. Therefore, PICO-dominated communities may be indicative for food web structures promoting a high degree of particle repackaging with potential for accelerated sinking velocities. Our $P_{\text{estimated}}$ -based interpretations (2, 3) align very well with the growing body of literature

pronouncing the important role of particle repackaging in particulate matter export [e.g., Lam et al., 2011; Henson et al., 2012b; Puigcorb  et al., 2015]. (4) Some of the highest sinking velocities were measured during a moderate *E. huxleyi* bloom toward the end of the experiment. This is in line with the common notion that CaCO₃ is a particularly effective ballast mineral and emphasizes the importance of *E. huxleyi* to support regional organic matter sequestration pulses.

Author Contributions

U.R. conceived, initiated, and organized the SOPRAN 2011 mesocosm study. L.T.B., T.B., and K.G.S. developed the subproject to study export of sinking material by means of sinking velocity measurements. L.T.B., T.B., A.L., N.H., and K.G.S. analyzed the data. L.T.B. interpreted the data and wrote the paper with comments from all coauthors.

Acknowledgments

We thank all participants of the 2011 SOPRAN mesocosm study, in particular, Signe Koch-Klavsen and Peter Fritzsche for measuring the chlorophyll *a*, BSI, and nutrient concentrations; Andrea Ludwig for the support on logistics and organization of the study; and Scarlett Sett, Jan B udenbender, Jan Czerny, Michael Sswat, Sonja Endres, Luisa Galgani, Hendrik Schultz, Christian Howe, Hubert Kraus, Allanah Paul, Aljosa Zavisic, Allison Webb, Rafael Bermudez, Jorun Egge, Barbara Niehoff, Daniela Freese, and Michael Meyerh ofer for their technical support. We are grateful to the crews of R/V *Alkor* (AL376), R/V *H akan Mosby* (2011609), and R/V *Heinke* (HE360) for the mooring and transportation of the mesocosms. This paper profited from the constructive comments from two anonymous reviewers. The project was funded by German Ministry for Science and Education (BMBF) in the framework of the SOPRAN and BIOACID projects with additional support (salary Aud Larsen) from the projects MicroPolar (RCN project 225956/E10) and MINOS (EU-ERC 250254). All data used here will be made available on www.pangaea.de and can also be requested directly from the corresponding author (lbach@geo-mar.de).

References

- Allredge, A. (1998), The carbon, nitrogen and mass content of marine snow as a function of aggregate size, *Deep Sea Res., Part I*, 45, 529–541, doi:10.1016/S0967-0637(97)00048-4.
- Allredge, A. L., and C. Gotschalk (1988), In situ settling behavior of marine snow, *Limnol. Oceanogr.*, 33(3), 339–351, doi:10.4319/lo.1988.33.3.0339.
- Alonso-Gonz alez, I. J., J. Aristeigui, C. Lee, A. Sanchez-Vidal, A. Calafat, J. Fabr es, P. Sangr a, P. Masqu e, A. Hern andez-Guerra, and V. Ben tez-Barrios (2010), Role of slowly settling particles in the ocean carbon cycle, *Geophys. Res. Lett.*, 37, L13608, doi:10.1029/2010GL043827.
- Armstrong, R. A., C. Lee, J. I. Hedges, S. Honjo, and S. G. Wakeham (2002), A new, mechanistic model for organic carbon fluxes in the ocean based on the quantitative association of POC with ballast minerals, *Deep Sea Res., Part II*, 49(1–3), 219–236.
- Armstrong, R. A., M. L. Peterson, C. Lee, and S. G. Wakeham (2009), Settling velocity spectra and the ballast ratio hypothesis, *Deep Sea Res., Part II*, 56(18), 1470–1478, doi:10.1016/j.dsr2.2008.11.032.
- Bach, L. T., U. Riebesell, S. Sett, S. Febir, P. Rzepka, and K. G. Schulz (2012a), An approach for particle sinking velocity measurements in the 3–400 µm size range and considerations on the effect of temperature on sinking rates, *Mar. Biol.*, 159(8), 1853–1864, doi:10.1007/s00227-012-1945-2.
- Bach, L. T., C. Bauke, K. J. S. Meier, U. Riebesell, and K. G. Schulz (2012b), Influence of changing carbonate chemistry on morphology and weight of coccoliths formed by *Emiliania huxleyi*, *Biogeosciences*, 9, 3449–3463, doi:10.5194/bg-9-3449-2012.
- Baker, E. T., H. B. Millburn, and D. A. Tennant (1988), Field assessment of sediment trap efficiency under varying flow conditions, *J. Mar. Res.*, 46, 573–592, doi:10.1357/002224088785113522.
- Balch, W. M., P. M. Holligan, S. G. Ackleson, and K. J. Voss (1991), Biological and optical properties of mesoscale coccolithophore blooms in the Gulf of Maine, *Limnol. Oceanogr.*, 36(4), 629–643, doi:10.4319/lo.1991.36.4.0629.
- Balch, W. M., K. Kilpatrick, P. M. Holligan, and T. Cucci (1993), Coccolith production and detachment by *Emiliania huxleyi* (*Prymnesiophyceae*), *J. Phycol.*, 29(5), 566–575.
- Berelson, W. M. (2001), The flux of particulate organic carbon into the ocean interior: A comparison of four U.S. JGOFS regional studies, *Oceanography*, 14(4), 59–67.
- Berelson, W. M. (2002), Particle settling rates increase with depth in the ocean, *Deep Sea Res., Part II*, 49, 237–251, doi:10.1016/S0967-0645(01)00102-3.
- Bienfang, P. K., P. J. Harrison, and L. M. Quarmby (1982), Sinking rate response to depletion of nitrate, phosphate and silicate in four marine diatoms, *Mar. Biol.*, 67, 295–302.
- Boxhammer, T., L. T. Bach, M. Nicolai, and U. Riebesell (2015), Video of a plankton community enclosed in a “Kiel Off-Shore Mesocosms for future Ocean Simulations” (KOSMOS) during the SOPRAN study in Raunefjord (Norway) 2011, doi:10.3289/KOSMOS_PLANKTON_NORWAY_2011.
- Boxhammer, T., L. T. Bach, J. Czerny, and U. Riebesell (2016), Technical Note: Sampling and processing of mesocosm sediment trap material for quantitative biogeochemical analysis, *Biogeosciences*, 13, 2, doi:10.5194/bg-12-18693-2015.
- Boyd, P. W., and T. W. Trull (2007), Understanding the export of biogenic particles in oceanic waters: Is there consensus?, *Prog. Oceanogr.*, 72(4), 276–312, doi:10.1016/j.pocan.2006.10.007.
- Bressac, M., C. Guieu, D. Doxaran, F. Bourrin, G. Obolensky, and J. M. Grisoni (2012), A mesocosm experiment coupled with optical measurements to assess the fate and sinking of atmospheric particles in clear oligotrophic waters, *Geo-Mar. Lett.*, 32, 153–164, doi:10.1007/s00367-011-0269-4.
- Burd, A. B., and G. A. Jackson (2009), Particle aggregation, *Annu. Rev. Mar. Sci.*, 1, 65–90, doi:10.1146/annurev.marine.010908.163904.
- Cavan, E. L., F. A. C. Le Moigne, A. J. Poulton, G. A. Tarling, P. Ward, C. J. Daniels, G. M. Fragoso, and R. J. Sanders (2015), Attenuation of particulate organic carbon flux in the Scotia Sea, Southern Ocean, is controlled by zooplankton fecal pellets, *Geophys. Res. Lett.*, 42, 821–830, doi:10.1002/2014GL062744.
- Clegg, S. L., and M. Whitfield (1990), A generalized model for the scavenging of trace metals in the open ocean—I. Particle cycling, *Deep-Sea Res., Part A*, 37(5), 809–832.
- Diercks, A.-R., and V. L. Asper (1997), In situ settling speeds of marine snow aggregates below the mixed layer: Black Sea and Gulf of Mexico, *Deep Sea Res., Part I*, 44(3), 385–398, doi:10.1016/S0967-0637(96)00104-5.
- Durkin, C. A., M. L. Estapa, and K. O. Buesseler (2015), Observations of carbon export by small sinking particles in the upper mesopelagic, *Mar. Chem.*, 175, 72–81, doi:10.1016/j.marchem.2015.02.011.
- Ebersbach, F., and T. W. Trull (2008), Sinking particle properties from polyacrylamide gels during the Kerguelen Ocean and Plateau compared Study (KEOPS): Zooplankton control of carbon export in an area of persistent natural iron inputs in the Southern Ocean, *Limnol. Oceanogr.*, 53(1), 212–224, doi:10.4319/lo.2008.53.1.0212.
- Engel, A., J. Szlosek, L. Abramson, Z. Liu, and C. Lee (2009), Investigating the effect of ballasting by CaCO₃ in *Emiliania huxleyi*: I. Formation, settling velocities and physical properties of aggregates, *Deep Sea Res., Part II*, 56, 1396–1407, doi:10.1016/j.dsr2.2008.11.027.
- Field, C. B., M. J. Behrenfeld, J. T. Randerson, and P. G. Falkowski (1998), Primary production of the biosphere: Integrating terrestrial and oceanic components, *Science*, 281(5374), 237–240, doi:10.1126/science.281.5374.237.

- Fischer, G., and G. Karakaş (2009), Sinking rates and ballast composition of particles in the Atlantic Ocean: Implications for the organic carbon fluxes to the deep ocean, *Biogeosciences*, *6*, 85–102, doi:10.5194/bg-6-85-2009.
- Francois, R., S. Honjo, R. Krishfield, and S. Manganini (2002), Factors controlling the flux of organic carbon to the bathypelagic zone of the ocean, *Global Biogeochem. Cycles*, *16*(4), 1087, doi:10.1029/2001GB001722.
- Giering, S. L. C., et al. (2014), Reconciliation of the carbon budget in the ocean's twilight zone, *Nature*, *507*(7493), 480–483, doi:10.1038/nature13123.
- Hansell, D. A., and C. A. Carlson (2001), Marine dissolved organic matter and the carbon cycle, *Oceanography*, *14*(4), 41–49.
- Hansen, H. P., and F. Koroleff (1999), Determination of nutrients, in *Methods of Seawater Analysis*, edited by K. Grasshoff, K. Kremling, and M. Ehrhardt, pp. 159–226, Wiley-VCH, Weinheim.
- Hedges, J. I., and J. M. Oades (1997), Comparative organic geochemistries of soils and marine sediments, *Org. Geochem.*, *27*(7-8), 319–361.
- Heldal, M., S. Norland, E. S. Erichsen, T. F. Thingstad, and G. Bratbak (2012), An unaccounted fraction of marine biogenic CaCO₃ particles, *PLoS One*, *7*(10), 1–6, doi:10.1371/journal.pone.0047887.
- Henson, S. A., R. Sanders, E. Madsen, P. J. Morris, F. Le Moigne, and G. D. Quartly (2011), A reduced estimate of the strength of the ocean's biological carbon pump, *Geophys. Res. Lett.*, *38*, 10–14, doi:10.1029/2011GL046735.
- Henson, S. A., R. Sanders, and E. Madsen (2012b), Global patterns in efficiency of particulate organic carbon export and transfer to the deep ocean, *Global Biogeochem. Cycles*, *26*, GB1028, doi:10.1029/2011GB004099.
- Henson, S., R. Lampitt, and D. Johns (2012a), Variability in phytoplankton community structure in response to the North Atlantic Oscillation and implications for organic carbon flux, *Limnol. Oceanogr.*, *57*(6), 1591–1601, doi:10.4319/lo.2012.57.6.1591.
- Hildebrandt, N. (2014), The response of three dominant Arctic copepod species to elevated CO₂ concentrations and water temperatures PhD thesis, 1–173 pp., Alfred-Wegener-Institut, Helmholtz-Zentrum für Polar- und Meeresforschung, Bremen.
- Holligan, P. M., et al. (1993), A biogeochemical study of the coccolithophore, *Emiliania huxleyi*, in the North Atlantic, *Global Biogeochem. Cycles*, *7*(4), 879–900, doi:10.1029/93GB01731.
- Honda, M. C., and S. Watanabe (2010), Importance of biogenic opal as ballast of particulate organic carbon (POC) transport and existence of mineral ballast-associated and residual POC in the Western Pacific Subarctic Gyre, *Geophys. Res. Lett.*, *37*, L02605, doi:10.1029/2009GL041521.
- Honjo, S., S. J. Manganini, R. A. Krishfield, and R. Francois (2008), Particulate organic carbon fluxes to the ocean interior and factors controlling the biological pump: A synthesis of global sediment trap programs since 1983, *Prog. Oceanogr.*, *76*(3), 217–285, doi:10.1016/j.pocean.2007.11.003.
- Hopkins, J., S. A. Henson, S. C. Painter, T. Tyrrell, and A. J. Poulton (2015), Phenological characteristics of global coccolithophore blooms, *Global Biogeochem. Cycles*, *29*, 239–253, doi:10.1002/2014GB004919.
- Jackson, G. A., D. M. Checkley, and M. Dagg (2015), Settling of particles in the upper 100 m of the ocean detected with autonomous profiling floats off California, *Deep Sea Res., Part I*, *99*, 75–86, doi:10.1016/j.dsr.2015.02.001.
- Kjørboe, T. (2001), Formation and fate of marine snow: Small-scale processes with large-scale implications, *Sci. Mar.*, *65*(2), 57–71.
- Klaas, C., and D. E. Archer (2002), Association of sinking organic matter with various types of mineral ballast in the deep sea: Implications for the rain ratio, *Global Biogeochem. Cycles*, *16*(4), 1116, doi:10.1029/2001GB001765.
- Kopelevich, O., V. Burenkov, S. Sheberstov, S. Vazyulya, M. Kravchishina, L. Pautova, V. Silkin, V. Artemiev, and A. Grigoriev (2014), Satellite monitoring of coccolithophore blooms in the Black Sea from ocean color data, *Remote Sens. Environ.*, *146*, 113–123, doi:10.1016/j.rse.2013.09.009.
- Lam, P. J., and J. K. B. Bishop (2007), High biomass, low export regimes in the Southern Ocean, *Deep Sea Res., Part II*, *54*, 601–638, doi:10.1016/j.dsr2.2007.01.013.
- Lam, P. J., S. C. Doney, and J. K. B. Bishop (2011), The dynamic ocean biological pump: Insights from a global compilation of particulate organic carbon, CaCO₃, and opal concentration profiles from the mesopelagic, *Global Biogeochem. Cycles*, *25*, GB3009, doi:10.1029/2010GB003868.
- Lampitt, R. S., K. F. Wishner, C. M. Turley, and M. V. Angel (1993), Marine snow studies in the Northeast Atlantic Ocean: Distribution, composition and role as a food source for migrating plankton, *Mar. Biol.*, *116*, 689–702, doi:10.1007/BF00355486.
- Larsen, A., T. Castberg, R. A. Sandaa, C. P. D. Brussaard, J. Egge, M. Heldal, A. Paulino, R. Thyraug, E. J. Van Hannen, and G. Bratbak (2001), Population dynamics and diversity of phytoplankton, bacteria and viruses in a seawater enclosure, *Mar. Ecol. Prog. Ser.*, *221*, 47–57, doi:10.3354/meps221047.
- Le Moigne, F. A. C., K. Pabortsava, C. L. J. Marcinko, P. Martin, and R. J. Sanders (2014), Where is mineral ballast important for surface export of particulate organic carbon in the ocean?, *Geophys. Res. Lett.*, *41*, 1–9, doi:10.1002/2014GL061678. Received
- Lieke, K. I., T. B. Kristensen, U. S. Korsholm, J. H. Sørensen, K. Kandler, S. Weinbruch, D. Ceburnis, J. Ovadnavaite, C. D. O'Dowd, and M. Bilde (2013), Characterization of volcanic ash from the 2011 Grímsvötn eruption by means of single-particle analysis, *Atmos. Environ.*, *79*, 411–420, doi:10.1016/j.atmosenv.2013.06.044.
- Lomas, M. W., D. K. Steinberg, T. Dickey, C. A. Carlson, N. B. Nelson, R. H. Condon, and N. R. Bates (2010), Increased ocean carbon export in the Sargasso Sea is countered by its enhanced mesopelagic attenuation, *Biogeosciences*, *7*, 57–70, doi:10.5194/bg-7-57-2010.
- Longhurst, A., S. Sathyendranath, T. Platt, and C. Caverhill (1995), An estimate of global primary production in the ocean from satellite radiometer data, *J. Plankton Res.*, *17*(6), 1245–1271.
- Maier-Reimer, E., U. Mikolajewicz, and A. Winguth (1996), Future ocean uptake of CO₂: Interaction between ocean circulation and biology, *Clim. Dyn.*, *12*(10), 711–722, doi:10.1007/s003820050138.
- Maiti, K., M. A. Charette, K. O. Buesseler, and M. Kahru (2013), An inverse relationship between production and export efficiency in the Southern Ocean, *Geophys. Res. Lett.*, *40*, 1557–1561, doi:10.1002/grl.50219.
- Martin, J. H., G. A. Knauer, D. M. Karl, and W. W. Broenkow (1987), VERTEX: Carbon cycling in the northeast Pacific, *Deep-Sea Res., Part A*, *34*(2), 267–285, doi:10.1016/0198-0149(87)90086-0.
- Martin, P., R. S. Lampitt, M. Jane Perry, R. Sanders, C. Lee, and E. D'Asaro (2011), Export and mesopelagic particle flux during a North Atlantic spring diatom bloom, *Deep Sea Res., Part I*, *58*(4), 338–349, doi:10.1016/j.dsr.2011.01.006.
- McDonnell, A. M. P., and K. O. Buesseler (2010), Variability in the average sinking velocity of marine particles, *Limnol. Oceanogr.*, *55*(5), 2085–2096, doi:10.4319/lo.2010.55.5.2085.
- McNown, J., and J. Malaika (1950), Effects of particle shape on settling velocity at low Reynolds numbers, *Eos Trans. AGU*, *31*, 74–82.
- Moore, J. K., and T. A. Villareal (1996), Size-ascent rate relationships in positively buoyant marine diatoms, *Limnol. Oceanogr.*, *41*(7), 1514–1520, doi:10.4319/lo.1996.41.7.1514.
- Moore, T. S., M. D. Dowell, and B. A. Franz (2012), Detection of coccolithophore blooms in ocean color satellite imagery: A generalized approach for use with multiple sensors, *Remote Sens. Environ.*, *117*, 249–263, doi:10.1016/j.rse.2011.10.001.

- Nowald, N., G. Fischer, V. Ratmeyer, M. Iversen, C. Reuter, and G. Wefer (2009), In-situ sinking speed measurements of marine snow aggregates acquired with a settling chamber mounted to the Cherokee ROV, in *Ocean. 2009-Europe*, pp. 1–6, IEEE, Bremen, doi:10.1109/OCEANSE.2009.5278186.
- Passow, U., and C. L. De La Rocha (2006), Accumulation of mineral ballast on organic aggregates, *Global Biogeochem. Cycles*, *20*, GB1013, doi:10.1029/2005GB002579.
- Pilskaln, C. H., C. Lehmann, J. B. Paduan, and M. W. Silver (1998), Spatial and temporal dynamics in marine aggregate abundance, sinking rate and flux: Monterey Bay, central California, *Deep Sea Res., Part II*, *45*(8-9), 1803–1837.
- Ploug, H., M. H. Iversen, and G. Fischer (2008), Ballast, sinking velocity, and apparent diffusivity within marine snow and zooplankton fecal pellets: Implications for substrate turnover by attached bacteria, *Limnol. Oceanogr.*, *53*(5), 1878–1886.
- Poulton, A. J., S. C. Painter, J. R. Young, N. R. Bates, B. Bowler, D. Drapeau, E. Lyczsckowski, and W. M. Balch (2013), The 2008 *Emiliania huxleyi* bloom along the Patagonian Shelf: Ecology, biogeochemistry, and cellular calcification, *Global Biogeochem. Cycles*, *27*, 1–11, doi:10.1002/2013GB004641.
- Puigcorb , V., C. R. Benitez-Nelson, P. Masqu , E. Verdeny, A. E. White, B. N. Popp, F. G. Prahl, and P. J. Lam (2015), Small phytoplankton drive high summertime carbon and nutrient export in the Gulf of California and eastern tropical North Pacific, *Global Biogeochem. Cycles*, *29*, 397–415, doi:10.1002/2014GB004979.
- Riebesell, U., et al. (2013), Technical note: A mobile sea-going mesocosm system—New opportunities for ocean change research, *Biogeosciences*, *10*(3), 1835–1847, doi:10.5194/bg-10-1835-2013.
- Sanders, R., et al. (2014), The biological carbon pump in the North Atlantic, *Prog. Oceanogr.*, *129*, 200–218, doi:10.1016/j.pcean.2014.05.005.
- Sarmiento, J. L., and N. Gruber (2006), *Ocean Biogeochemical Dynamics*, Princeton Univ. Press, Princeton.
- Schmidt, K., C. L. De La Rocha, M. Gallinari, and G. Cortese (2014), Not all calcite ballast is created equal: Differing effects of foraminiferan and coccolith calcite on the formation and sinking of aggregates, *Biogeosciences*, *11*, 135–145, doi:10.5194/bg-11-135-2014.
- Schmittner, A., A. Oschlies, H. D. Matthews, and E. D. Galbraith (2008), Future changes in climate, ocean circulation, ecosystems, and biogeochemical cycling simulated for a business-as-usual CO₂ emission scenario until year 4000 AD, *Global Biogeochem. Cycles*, *22*, GB1013, doi:10.1029/2007GB002953.
- Schulz, K. G., et al. (2013), Temporal biomass dynamics of an Arctic plankton bloom in response to increasing levels of atmospheric carbon dioxide, *Biogeosciences*, *10*, 161–180, doi:10.5194/bg-10-161-2013.
- Sharqawy, M. H., J. H. Lienhard, and S. M. Zubair (2010), Thermophysical properties of seawater: A review of existing correlations and data, *Desalin. Water Treat.*, *16*, 354–380.
- Siegel, D. A., K. O. Buesseler, S. C. Doney, S. F. Sailley, M. J. Behrenfeld, and P. W. Boyd (2014), Global assessment of ocean carbon export by combining satellite observations and food-web models, *Global Biogeochem. Cycles*, *28*, 181–196, doi:10.1002/2013GB004743.
- Smayda, T. J. (1970), The suspension and sinking of phytoplankton in the sea, in *Oceanography and Marine Biology: An Annual Review*, pp. 353–414, Taylor and Francis, London.
- Smetacek, V., et al. (2012), Deep carbon export from a Southern Ocean iron-fertilized diatom bloom, *Nature*, *487*(7407), 313–319, doi:10.1038/nature11229.
- Steinberg, D. K., B. A. S. Van Mooy, K. O. Buesseler, P. W. Boyd, T. Kobari, and D. M. Karl (2008), Bacterial vs. zooplankton control of sinking particle flux in the ocean's twilight zone, *Limnol. Oceanogr.*, *53*(4), 1327–1338, doi:10.4319/lo.2008.53.4.1327.
- Stokes, G. G. (1850), On the effect of the internal friction of fluids on the motion of pendulums, *Trans. Cambridge Philos. Soc.*, *9*, 1–86.
- Tesche, M., P. Glantz, C. Johansson, M. Norman, A. Hiebsch, A. Ansmann, D. Althausen, R. Engelmann, and P. Seifert (2012), Volcanic ash over Scandinavia originating from the Gr msv tn eruptions in May 2011, *J. Geophys. Res.*, *117*, D09201, doi:10.1029/2011JD017090.
- Turner, J. T. (2002), Zooplankton fecal pellets, marine snow and sinking phytoplankton blooms, *Aquat. Microb. Ecol.*, *27*, 57–102.
- Volk, T., and M. I. Hoffert (1985), Ocean carbon pumps: Analysis of relative strengths and efficiencies in ocean-driven atmospheric CO₂ changes, in *The Carbon Cycle and Atmospheric CO₂: Natural Variations Archaean to Present*, vol. 32, edited by E. T. Sundquist and W. S. Broecker, pp. 99–110, AGU, Washington, D. C.
- Waite, A. M.,  . Gustafsson, O. Lindahl, and P. Tiselius (2005), Linking ecosystem dynamics and biogeochemistry: Sinking fractionation of organic carbon in a Swedish fjord, *Limnol. Oceanogr.*, *50*(2), 658–671, doi:10.4319/lo.2005.50.2.0658.
- Welschmeyer, N. (1994), Fluorometric analysis of chlorophyll *a* in the presence of chlorophyll *b* and pheopigments, *Limnol. Oceanogr.*, *39*(8), 1985–1992.
- Wilson, J. D., S. Barker, and A. Ridgwell (2012), Assessment of the spatial variability in particulate organic matter and mineral sinking fluxes in the ocean interior: Implications for the ballast hypothesis, *Global Biogeochem. Cycles*, *26*, GB4011, doi:10.1029/2012GB004398.
- Xue, J., and R. A. Armstrong (2009), An improved “benchmark” method for estimating particle settling velocities from time-series sediment trap fluxes, *Deep Sea Res., Part II*, *56*, 1479–1486, doi:10.1016/j.dsr2.2008.11.033.
- Yasumoto, K., et al. (2014), Biogenic polyamines capture CO₂ and accelerate extracellular bacterial CaCO₃ formation, *Mar. Biotechnol.*, *16*, 465–474, doi:10.1007/s10126-014-9566-z.